arXiv:1607.02471v1 [cond-mat.supr-con] 8 Jul 2016

Multiple quantum phase transitions and superconductivity in Ce-based heavy fermions

Z. F. Weng,[1] M. Smidman,[1] L. Jiao,[1] Xin Lu,[1,2,*] and H. Q. Yuan[1,2,†]

[1] *Center for Correlated Matter and Department of Physics, Zhejiang University, Hangzhou 310058, China*
[2] *Collaborative Innovation Center of Advanced Microstructures, Nanjing 210093, China*

(Dated: July 11, 2016)

Heavy fermions have served as prototype examples of strongly-correlated electron systems. The occurrence of unconventional superconductivity in close proximity to the electronic instabilities associated with various degrees of freedom points to an intricate relationship between superconductivity and other electronic states, which is unique but also shares some common features with high temperature superconductivity. The magnetic order in heavy fermion compounds can be continuously suppressed by tuning external parameters to a quantum critical point, and the role of quantum criticality in determining the properties of heavy fermion systems is an important unresolved issue. Here we review the recent progress of studies on Ce based heavy fermion superconductors, with an emphasis on the superconductivity emerging on the edge of magnetic and charge instabilities as well as the quantum phase transitions which occur by tuning different parameters, such as pressure, magnetic field and doping. We discuss systems where multiple quantum critical points occur and whether they can be classified in a unified manner, in particular in terms of the evolution of the Fermi surface topology.

INTRODUCTION

As prototype examples of strongly correlated electron systems, heavy fermions have been intensively investigated since their discovery due to their exotic properties and fascinating underlying physics [1–8]. The discovery of unconventional superconductivity in the heavy fermion compound $CeCu_2Si_2$ with $T_c \simeq 0.6$ K by Frank Steglich in 1979 [9] pioneered research into unconventional superconductivity and in particular, the intricate relationship between superconductivity and magnetism, which had been previously considered to be antagonistic [4, 5]. Understanding the close relationship between superconductivity and quantum criticality may be important for solving the puzzles of high-temperature superconductivity in cuprate or iron pnictide superconductors, but its underlying mechanism still remains as an intriguing open issue [10–13].

Heavy fermion systems generally refer to certain intermetallic compounds containing either lanthanide (Ce, Yb, Pr, etc.) or actinide (U, Pu, Np, etc.) elements. Electrons from partially filled $4f$ or $5f$ orbits are arranged in a periodic lattice and interact with the itinerant conduction electrons, which leads to many emergent quantum phenomena. Among them, Ce-based compounds serve as the simplest examples to demonstrate much of the important heavy fermion physics, since each Ce atom has only one f electron, with an atomic configuration $4f^1(5d6s^2)$. Elemental Ce shows a discontinuous valence transition from a Ce valence of 3.03 (γ phase) to 3.14 (α phase) at 300 K [15], while Ce-based materials display a variety of ground states such as magnetic ordering, heavy Fermi liquid state or mixed-valence state. Due to the relatively small energy scales in heavy fermion systems, the ground state can often be readily tuned by external parameters such as pressure, magnetic fields or chemical doping. For example, the antiferromagnetism (AFM) can be continuously suppressed by applying pressure or a magnetic field in $CeRhIn_5$ [16–18], pressure in $CePd_2Si_2$ [10] or by doping in $CeCu_{6-x}Au_x$ [19]. Moreover, charge degrees of freedom increasingly need to be taken into account upon enhancing the hybridization between the f and conduction electrons, leading to valence instabilities or crossover behavior, as shown in the schematic phase diagram in Fig. 1 [14]. Unconventional superconductivity (SC) occurs when the system is on the verge of either magnetic or valence-instabilities [14], suggesting a close relationship between the SC and the asso-

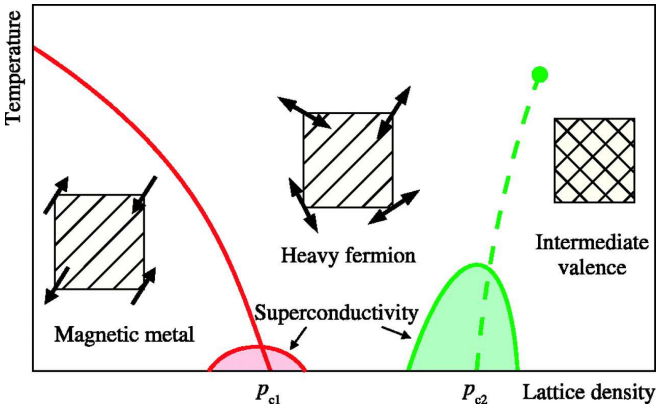

FIG. 1: Schematic phase diagram of Ce-based narrow band metals. Upon increasing the hybridization by applying pressure, the ground state changes from an antiferromagnetic to heavy fermion state, before entering the intermediate valence regime. Two critical points associated with spin and valence instabilities occur at p_{c1} and p_{c2} respectively, around which there is unconventional superconductivity. Reprinted with permission from Ref. [14]. Copyright 2003 AAAS.

ciated critical fluctuations. Presently, almost half of the heavy fermion superconductors which have been found are Ce-based compounds, some of which are superconducting at ambient pressure, while others require high pressures to be applied.

Studies of quantum criticality and superconductivity raise a series of important questions with regards to strongly correlated electron systems: (1) whether there exist distinctly different types of quantum critical points (QCP) and whether these can be universally classified; (2) the possibility of multiple QCPs upon tuning with different parameters and the validity of the global phase diagram; (3) the underlying pairing mechanisms of heavy fermion superconductivity and its relationship to the QCP. The remainder of the review is organised as follows. Firstly we will give a brief overview of various aspects of heavy fermion physics and quantum criticality. We will then discuss examples of systems which become superconducting near an antiferromagnetic instability before discussing the possibility of superconductivity occurring in proximity to valence transitions. Here we present some examples of systems where a parameter such as pressure may tune the system through multiple instabilities, corresponding to different degrees of freedom. We then review some materials which display multiple quantum phase transitions, where distinctly different behaviors are seen when the system is tuned by different parameters. Finally we will discuss to what extent these behaviors can be classified in a universal manner and the applicability of the recently proposed global phase diagram [20–22] for heavy fermion systems.

THEORETICAL APPROACHES FROM HEAVY FERMION TO MIXED VALENCE STATE

Kondo vs. RKKY Interaction

Many Ce based systems can be modelled as a lattice of f electrons, which antiferromagnetically couple with the conduction electrons via the Kondo interaction. This is the Kondo lattice model given by [23]

$$H = \sum_{k\sigma} \epsilon_k c^+_{k\sigma} c_{k\sigma} + J \sum_i \overrightarrow{\sigma}(i) \cdot \overrightarrow{S}_i; \qquad (1)$$

where J characterizes the coupling strength between the spin density of the conduction electrons $\overrightarrow{\sigma}(i)$ and the f electron spin $\overrightarrow{S}_i$ at the site i. In the canonical Kondo impurity problem, as the temperature reduces the localized f moments are compensated by the opposite spins of the conduction electrons. Below the characteristic Kondo temperature T_K, a Kondo singlet state forms [7, 24], giving rise to a logarithmic increase in the resistivity due to the enhanced scattering of conduction electrons. The effect of the f electrons being arranged in a periodic lattice, means that upon reducing the temperature further, the electrical resistivity $\rho(T)$ typically reaches a maximum, before decreasing rapidly. This characteristic temperature is commonly called the coherence temperature, below which Kondo scattering becomes coherent and the system evolves into a state that shows Landau Fermi liquid behavior [8, 25]. However, the renormalized electron mass is much larger than that of free electrons due to the hybridization between localized electrons and conduction electrons. The term "heavy fermion" has therefore been coined to distinguish the behavior of these materials from that of a normal Fermi liquid in metals [1].

Besides the Kondo interaction, there also exists a competing interaction in heavy fermion systems, the Ruderman-Kittel-Kasuya-Yosida (RKKY) interaction [26–28]. While the Kondo interaction screens the magnetic moments of localized f electrons and leads to the formation of a heavy Fermi-liquid state, the RKKY interaction favors long-range magnetic order. Here the localized electrons can polarize the surrounding conduction electrons to form a spin density wave in space, which interacts with other f electrons leading to an ordered state. The temperatures characterizing the Kondo interaction (T_K) and RKKY interaction (T_{RKKY}) can both be expressed in terms of the interaction J between the f and conduction electrons and the density of states at the Fermi energy $D(E_F)$, but they follow different behaviors [23]. The Kondo temperature scales as

$$T_K \propto \exp(-\frac{1}{JD(E_F)}); \qquad (2)$$

while the RKKY temperature follows

$$T_{RKKY} \propto D(E_F)J^2. \qquad (3)$$

Magnetic quantum criticality

The competition between the Kondo and RKKY interactions in heavy fermion systems may result in various ground states, leading to a rich phase diagram, which can be qualitatively described by the Doniach phase diagram as schematically shown in Fig. 2 [23]. The hybridization constant J can be effectively tuned by pressure, chemical doping or magnetic field because the associated energy scales are relatively small in heavy fermion compounds. When J is small, the RKKY interaction becomes dominant and the system exhibits a magnetically ordered ground state, such as antiferromagnetism. With increasing hybridization, the Kondo interaction is enhanced and the system may exhibit heavy fermion behavior. At a critical value J_c, the system may experience a continuous phase transition at zero temperature, *i.e.*, a QCP, changing the ground state from a magnetically ordered state to a disordered state, which is driven by quantum fluctuations instead of thermal fluctuations. Near the quantum

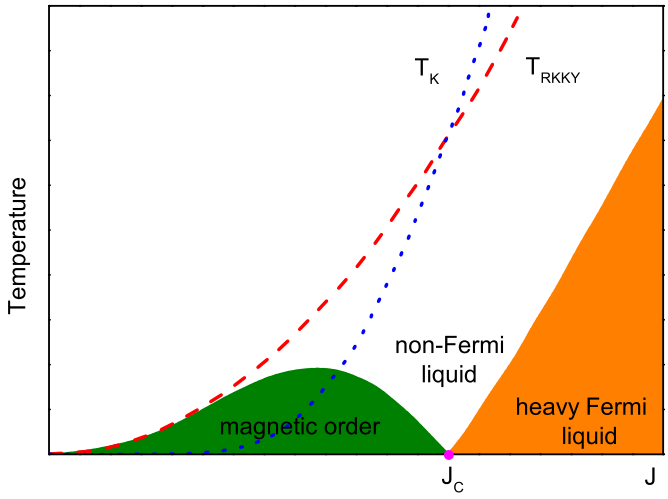

FIG. 2: A schematic plot of the Doniach phase diagram for heavy fermion systems [23], where there is competition between the RKKY interaction and Kondo interaction, with relative strengths T_{RKKY} and T_K respectively.

critical point of heavy fermion compounds, exotic quantum states and anomalous normal-state behavior have been widely observed [1–8]. For example, the specific heat C/T can diverge logarithmically and the resistivity may show a linear rather than quadratic temperature dependence as the temperature approaches zero.

The universality of the critical behaviors and its underlying mechanism remain unresolved. It was proposed that QCPs in heavy fermion compounds can be categorized into two types: conventional spin-density-wave [29–31] or unconventional Kondo breakdown (local) QCPs [32–34], where in the latter case, the Fermi surface topology should be taken into consideration in addition to order parameter fluctuations. In the Kondo lattice, whether f electrons contribute to the Fermi surface volume depends on the degree of Kondo screening. There exists a characteristic energy scale line E^*_{loc} at low temperatures, signaling a change from a small Fermi surface volume to a large Fermi surface volume, which is a crossover at finite temperatures, but a sharp transition at zero temperature. In the case of a Kondo-breakdown QCP, the E^*_{loc} line terminates exactly where the ordering temperature T_N vanishes and as a result, the critical fluctuations are associated with not only the order parameter but also drastic changes of the Fermi surface volume [32, 33]. On the other hand, when E^*_{loc} and T_N intersect at a finite temperature, the long-range magnetic order switches from local moment magnetism, with a small Fermi surface volume(AF_S) to an itinerant spin-density-wave with a large Fermi surface volume (AF_L) [35]. The ordering is then completely suppressed at the QCP, where only magnetic order parameter fluctuations are present and beyond this the system is paramagnetic, with a large FS (P_L). This scenario is generally referred to as a spin-density-wave QCP, with behavior consistent with the predictions from conventional Hertz-Millis models [29–31].

Periodic Anderson model

The periodic Anderson lattice model is the basic model for heavy fermion systems [7, 8, 36], which gives a microscopic picture for understanding the various possible ground states:

$$H = \sum_{k\sigma} \epsilon_k c^+_{k\sigma} c_{k\sigma} + \epsilon_f \sum_{i\sigma} n^f_{i\sigma} + U \sum_i n^f_{i\uparrow} n^f_{i\downarrow} + V \sum_{i\sigma} \{f^+_{i\sigma} c_{i\sigma} + h.c.\}, \quad (4)$$

where $H_c = \sum_{k\sigma} \epsilon_k c^+_{k\sigma} c_{k\sigma}$ is the conduction electron energy, $H_f = \epsilon_f \sum_{i\sigma} n^f_{i\sigma} + U \sum_i n^f_{i\uparrow} n^f_{i\downarrow}$ contains the f electron energy in the first term and the onsite Coulomb repulsion U between electrons of opposite spins in the second term, and $H_{hyb} = V \sum_{i\sigma} \{f^+_{i\sigma} c_{i\sigma} + h.c.\}$ represents the hybridization between the f and conduction electrons.

Many features of heavy fermion systems can be understood by considering a model with a single f electron, the Anderson impurity model [36]. Here the f electron can be either in the $|f^1_\uparrow\rangle$ or the $|f^1_\downarrow\rangle$ state [8]. The energy cost of losing this electron to leave a vacant $|f^0\rangle$ state is $-\epsilon_f$, while $\epsilon_f + U$ is the energy for gaining an extra electron, to give a doubly occupied $|f^2\rangle$ state. In the heavy fermion regime, real charge fluctuations associated with transitions from $|f^1\rangle$ to the $|f^0\rangle$ or $|f^2\rangle$ states are eliminated and the Ce valence remains integer. However, virtual processes render an effective antiferromagnetic interaction between the conduction electrons and local f moment in the form of the Kondo interaction $H_K = J\overrightarrow{\sigma}(0) \cdot \overrightarrow{S}_f$, with a coupling strength $J = V^2[\frac{1}{U+\epsilon_f} + \frac{1}{|\epsilon_f|}]$ [37]. Similarly, the periodic Anderson model can be transformed into the Kondo lattice model given by Eq. 1.

Upon either increasing the hybridization V between localized f and conduction electrons or shifting the f electron level ϵ_f closer to the Fermi energy E_F, valence fluctuations can no longer be neglected and the local moment approximation is not valid. The system smoothly evolves into the intermediate valence (mixed-valence) regime, where the Ce valence is not close to the trivalent integer limit [8]. The electronic specific heat coefficient monotonically decreases with increasing V, due to a reduced effective electron mass and the Curie-Weiss type behavior of the magnetic susceptibility is gradually suppressed with the disappearance of local moments.

Valence Instability based on the generalized periodic Anderson lattice model

In the Anderson lattice model, there is a smooth crossover from the heavy fermion to intermediate valence state. However, it has been proposed that the valence transitions or sharp valence crossovers observed in several heavy fermion systems can be understood from a generalized periodical Anderson lattice model [38]:

$$H = H_c + H_f + H_{hyb} + U_{fc} \sum_{i\sigma\sigma'} n^f_{i\sigma} n^c_{i\sigma'}, \qquad (5)$$

where the additional term with U_{fc} represents the strength of the local Coulomb repulsion between the f and conduction electrons. Using the mean-field approximation with the slave-boson formalism, it was demonstrated that as ε_f moves towards the Fermi level, a drastic change of the Ce valence may take place at $\epsilon_f \sim E_F - U_{fc}$ [38], where the $|f^0\rangle$ and $|f^1\rangle$ states are degenerate with enhanced valence fluctuations, assuming that U_{fc} is of the order of the bandwidth of the conduction band [38, 39]. As shown in Fig. 3(a) [39], there exists a first-order valence transition (FOVT) line in the schematic phase diagram of the U_{fc}-ϵ_f plane, which terminates at a quantum critical end point (QCEP) and is connected to a sharp valence crossover region [38, 39]. Adiabatic continuation between the Kondo and mixed-valence state can be achieved by avoiding the QCEP of the first-order transition line as in the liquid-gas case. In the temperature-U_{fc}-ϵ_f phase diagram shown in Fig. 3(b) [39], the surface cuts (A) and (B) respectively represent possible scenarios for the pressure induced behavior of Ce metal with a FOVT and Ce-based compounds with a sharp valence crossover.

At the critical valence transition, a few predictions have been made based on this model: [38, 40, 41] (1) a linear temperature dependence of the electrical resistivity; (2) an enhancement of the impurity scattering leading to a maximum in the residual resistivity; (3) a dramatic decrease of electronic scattering, as reflected in the resistivity coefficient A, due to the sharp valence change between the Kondo and intermediate valence regimes. (4) In addition, a d-wave superconducting state may be stabilized by the significantly enhanced valence fluctuations, with T_c reaching a maximum value.

The typical phase diagram of Ce-based heavy fermion systems may be summarized by Fig. 1 [14]. Upon increasing the hybridization, e.g. by applying pressure, the long range antiferromagnetic order is eventually suppressed and a heavy fermion state develops. Near the AFM QCP, heavy fermion superconductivity is often observed. Upon further increasing the hybridization, the charge degrees of freedom may now play an important role and the system is driven into a mixed-valence state. Here the Coulomb interaction between f and conduction electrons may lead to either a valence transition or crossover and superconductivity may also appear in proximity to the valence instability.

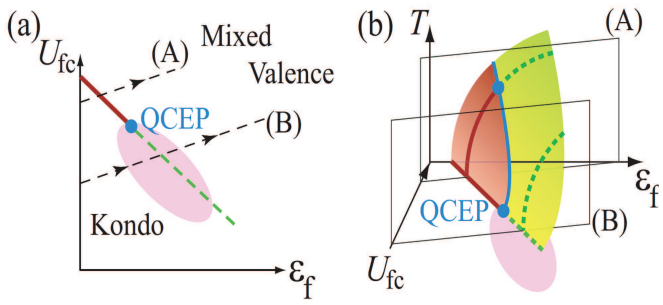

FIG. 3: (a) Schematic phase diagram of the ground states of the generalized periodic Anderson lattice model in the U_{fc}-ϵ_f plane, where local Kondo and mixed valence regions are separated by a first-order valence transition (FOVT) line, which terminates at a quantum critical end point (QCEP). Lines (A) and (B) represent routes with a FOVT and continuous crossover behavior respectively. (b) Schematic $T - U_{fc} - \epsilon_f$ phase diagram derived from the generalized periodic Anderson lattice model, which extends (a) to finite temperatures. Adapted with permission from Ref. [39]. Copyright 2011 the Institute of Physics.

SUPERCONDUCTIVITY NEAR A MAGNETIC INSTABILITY

As has been discussed previously, with increased coupling J, the strength of the Kondo interaction becomes greater than that of the RKKY interaction, which leads to the suppression of magnetic order at a QCP. In many Ce based heavy fermion systems, superconductivity emerges in the vicinity of this suppression. Examples of heavy fermion superconductors and their physical properties are displayed in Table. I, where in some instances the system is superconducting at ambient pressure, while in other cases pressure must be applied for superconductivity to be realized. The phase diagrams of many Ce-based heavy fermion superconductors are similar to that depicted in Fig. 4(a). In the vicinity of an AFM QCP, non-Fermi liquid behavior in the normal state above T_c is generally observed in the resistivity and specific heat, due to enhanced quantum critical spin fluctuations. Heavy Fermi liquid behavior is recovered upon crossing the QCP, below a characteristic Fermi liquid temperature T_{FL}, which increases with increasing pressure.

The close relationship between superconductivity and magnetism in heavy fermion systems is in stark contrast to conventional BCS superconductors, where the presence of magnetism is generally considered to be antagonistic to superconductivity. However, the presence of superconductivity on the border of a magnetic instabil-

TABLE I: Physical properties of Ce-based heavy fermion superconductors.

Compound	Crystal Structure	γ [J/(mol K^2)]	T_N(p = 0) (K)	Propagation vector Q	p_c (GPa)	T_c (K)	H_{c2}(//c) (T)	H_{c2}($\perp$c) (T)
$CePd_2Si_2$	I4/mmm	0.11 [42]	10 [42]	(1/2, 1/2, 0) [43]	2.8 [10]	0.5 [10]	1.3	0.7 [44]
$CeNi_2Ge_2$	I4/mmm	0.35 [45]	-	-	-	0.2 [46]		
$CeRh_2Si_2$	I4/mmm	0.0228 [47]	36 [48]	(1/2, 1/2, 0) (1/2, 1/2, 1/2) ($T < 25$ K) [43]	1.06 [49]	0.4 [49]	0.28 [49]	
$CeCu_2Si_2$	I4/mmm	1 [9]	0.8 [50]	(0.215, 0.215, 0.53) [51]	-	0.6 [52]	2.4	2 [52]
$CeCu_2Ge_2$	I4/mmm	0.1 [53]	4.15 [53]	(0.28, 0.28, 0.54) [54]	10.1 [55]	0.64 [55]	2 [55]	
$CeAu_2Si_2$	I4/mmm	0.011 [56]	10 [43]	(0, 0, 0) [43]	22.5 [57]	2.5 [57]	9.2 [57]	
$CePt_2In_7$	I4/mmm	0.34 [58]	5.5 [58]	-	3.5 [58]	2.1 [58]	15 [59]	-
$CeIn_3$	Pm3m	0.12 [60]	10.23 [61]	(1/2, 1/2, 1/2) [62]	2.65 [63]	0.204 [63]	0.45 [64]	
$CeCoIn_5$	P4/mmm	0.29 [65]	-	-	-	2.3 [65]	5.2	11.5 [66]
$CeRhIn_5$	P4/mmm	0.4 [67]	3.8 [67]	(1/2, 1/2, 0.297) [68]	2.3 [16]	2.258 [69]	16.9	9.7 [70]
$CeIrIn_5$	P4/mmm	0.72 [71]	-	-	-	0.4 [71]	2.3	7 [71]
Ce_2CoIn_8	P4/mmm	0.5 [72]	-	-	-	0.4 [72]	0.9	1.1 [73]
Ce_2RhIn_8	P4/mmm	0.4 [74]	2.8 [74]	(1/2, 1/2, 0) [75]	2.3 [76]	2 [76]	5.36 [76]	
Ce_2PdIn_8	P4/mmm	1 [77]	10 [77]	-	-	0.68 [77]	2.2	1.8 [78]
$CePt_3Si$	P4mm	0.39 [79]	2.2 [79]	(0, 0, 1/2) [80]	-	0.75 [79]	3.2	2.7 [81]
$CeCoGe_3$	I4mm	0.111 [82]	21 [82]	(0, 0, 1/2) ($T < 8$ K) [83]	5.5 [84]	0.7 [84]	24	3.1 [85]
$CeRhSi_3$	I4mm	0.12 [86]	1.6 [87]	($\pm$0.215, 0, 0.5) [88]	2.36 [89]	1.1 [87]	30	7 [90]
$CeIrSi_3$	I4mm	0.125 [86]	5 [86]	($\pm$0.265, 0, 0.43) [91]	2.5 [92]	1.6 [92]	45	9.5 [93]
$CeIrGe_3$	I4mm	0.08 [86]	8.7 [86]	-	20 [94]	1.5 [94]	> 10 [94]	-

ity is also commonly found in other unconventional superconductors such as cuprate, iron-based and organic superconductors [95], as shown in Fig. 4. The nature of the antiferromagnetically ordered parent compound varies, with Mott insulating, semi-metallic or intermetallic behavior observed, yet in all cases the superconductivity is in the vicinity of magnetism. Even though the T_c of heavy fermion superconductors is usually much lower than cuprate or iron-based superconductors, the ratio T_c/T_F is much higher than BCS superconductors [9]. This is because the effective Fermi temperature T_F is much smaller, on the order of the coherence temperature, compared to $\sim 10^4$ K in simple metals. In this sense, heavy fermion superconductors may also be regarded as analogous to the high T_c materials.

In a simple phenomenological model [11], the spin interaction between quasiparticles can be given by

$$V_{ind}(r,t) = -s \cdot s' g_m^2 \chi_m(r,t), \tag{6}$$

where g_m characterizes the coupling strength of the spins s and s', while $\chi_m(r,t)$ is the non-local magnetic susceptibility. On the border of AFM long-range order, $\chi_m(r,t)$ is expected to be dramatically enhanced due to quantum fluctuations and to oscillate in real space, giving the attractive interaction necessary for the formation of Cooper pairs in spin-singlet states with non-zero angular momentum, such as d-wave superconductivity. However, experimentally characterizing the pairing symmetry of many heavy fermion superconductors remains a challenge. In particular, for those systems where superconductivity requires high pressures and very low temperatures, the range of experimental techniques available for measuring the pairing symmetry is greatly reduced. Also in noncentrosymmetric heavy fermion superconductors [79], the effects of inversion symmetry breaking and antisymmetric spin-orbit coupling need to be taken into account, which will generally lead to very different pairing states with a mixture of singlet and triplet components [96].

While the presence of superconductivity on the border of magnetism is well established for heavy fermion superconductors, the detailed relationship between superconductivity, AFM order and quantum criticality in different systems is the subject of much ongoing interest. There are particular questions about the degree of competition or coexistence between magnetism and superconductivity in these systems and the extent to which magnetism persists within the superconducting dome. In addition, the role of quantum criticality in driving superconductivity is not well understood, particularly in those systems where there is evidence for a first-order transition between the AFM and paramagnetic states and a lack of evidence for enhanced critical fluctuations. In the remainder of this section, we describe in detail the properties of several heavy fermion superconductors, with a particular focus on the relationship between superconductivity and magnetic order and the nature of the superconducting phases which emerge.

Superconductivity near an antiferromagnetic QCP

$CeCu_2Si_2$ was the first heavy fermion system [9] found to be superconducting and the ground state can be categorized as A-, A/S- or S-type, where A and S denote an-

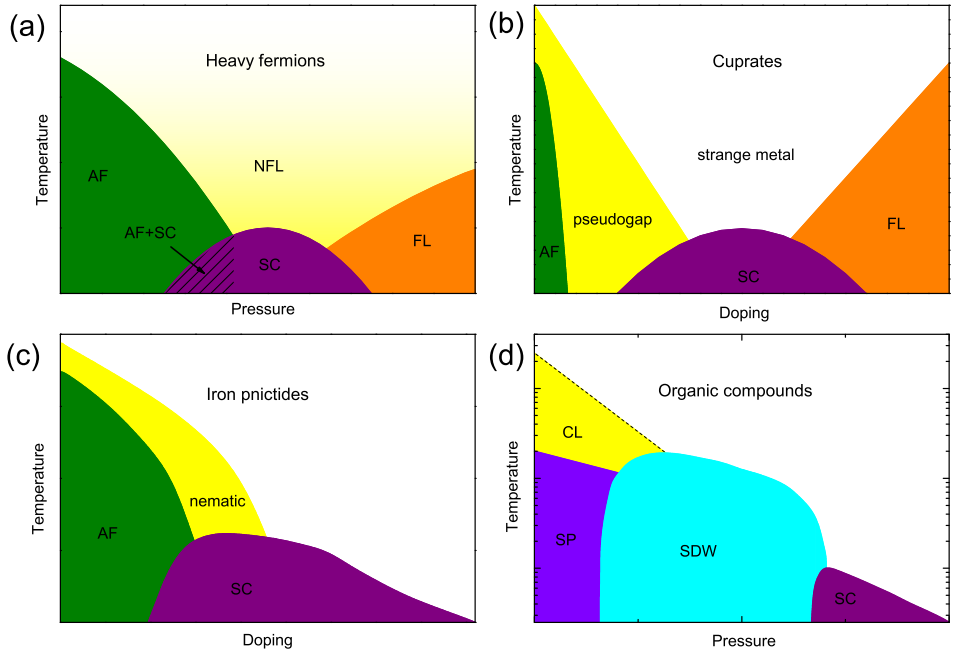

FIG. 4: Phase diagrams for (a) heavy fermions (b) cuprates (c) iron pnictides and (d) organic compounds [95]. All of the diagrams show several similar features.

tiferromagnetism and superconductivity [97] respectively. A schematic phase diagram is displayed in Fig. 5 [98], where at ambient pressure the hybridization tuning parameter J depends on the precise Cu composition [99] and J is increased by applying pressure. Upon tuning J through a QCP, the magnetism is entirely suppressed and only a superconducting transition is observed. The A-type samples order antiferromagnetically at T_N and may also display superconductivity at a much lower T_c, while S-type samples display only superconductivity. On the other hand in A/S-type samples, both antiferromagnetic and superconducting transitions are detected with similar values of T_N and T_c. The antiferromagnetic phase consists of incommensurate SDW order with a propagation vector $\mathbf{q} = (0.215, 0.215, 0.530)$ and a magnetic moment of $\sim 0.1\ \mu_B$/Ce [51]. Muon spin relaxation (μSR) measurements [100, 101] of A/S-type samples show that upon entering the superconducting state, the magnetic volume fraction decreases, indicating there is competition between magnetism and superconductivity and a separation of the two phases on a microscopic level.

Despite experimental efforts, the superconducting gap structure and pairing symmetry, which are closely related to the pairing mechanism, still remain controversial and are the subject of debate. It was generally believed that the gap symmetry of $CeCu_2Si_2$ should be even parity d-wave with line nodes. The even parity is a consequence of spin-singlet superconductivity, which was inferred from both the evidence for Pauli paramagnetic limiting of the upper critical field H_{c2} [102] and a decrease of the NMR Knight shift below T_c [103]. As shown in Fig. 6(b), the presence of line nodes was supported by both a T^3 dependence and the absence of a coherence peak in the spin lattice relaxation rate $1/T_1$ from NQR measurements [104, 105]. Inelastic neutron scattering and the subsequent theoretical analysis suggested $d_{x^2-y^2}$ symmetry for $CeCu_2Si_2$ [51, 106], while the four-fold oscillations observed in the angular dependence of H_{c2} are consistent with d_{xy} symmetry [107]. However, recent low-temperature specific heat measurements of $CeCu_2Si_2$ exhibit an exponential temperature dependence (Fig. 6(a)), characteristic of fully gapped superconductivity [108]. In addition, both the recent specific heat [108] and scanning tunneling spectroscopy [109] measurements also indicate the presence of multiple superconducting gaps . An alternative loop nodal $s\pm$ pairing symmetry was proposed [110]. However, it is difficult to explain the results of inelastic neutron scattering measurements [98] using either the isotropic two-band s-wave or loop nodal $s\pm$ scenarios, since they do not provide the deduced sign change of the superconducting gap between regions of the Fermi surface spanned by the antiferromagnetic ordering wave vector. Recent penetration depth measurements also support the presence of fully gapped superconductivity and we propose a fully-gapped $d + d$ band-mixing pairing state, which changes sign over the Fermi surface and therefore appears to be consistent with the literature results [111].

A number of additional heavy fermion superconductors have also been discovered. $CeIn_3$ is antiferromagnetic,

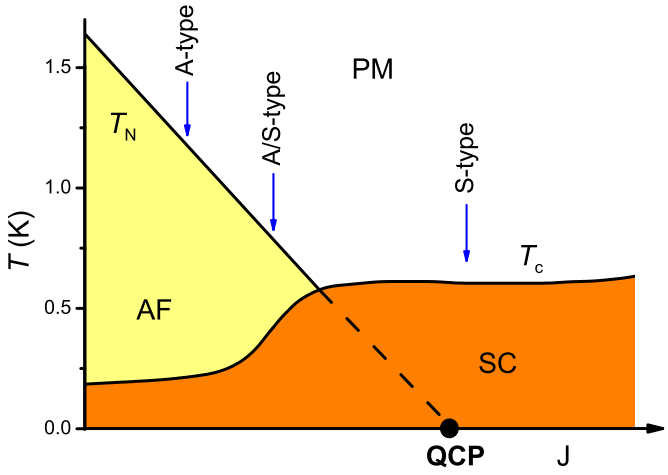

FIG. 5: Schematic phase diagram of $CeCu_2Si_2$ [98], where the parameter J can be tuned either by applying pressure, or by small changes to the composition.

with $T_N \sim 10$ K at ambient pressure, but the magnetism is entirely suppressed by applying a pressure of around 2.6 GPa [63]. Superconductivity emerges near the region where the suppression occurs, with a maximum T_c less than 0.3 K. NQR measurements [112] in the superconducting state when magnetism has been suppressed show a lack of a coherence peak and a T^3 dependence of $1/T_1$. These observations indicate that there are line nodes in the superconducting gap. Introducing a buffer layer $M\mathrm{In}_2$ (M = Co, Rh or Ir) into the superconducting block CeIn_3 lead to the discovery of the so called 115 family [113, 114], which have become an important family of heavy fermion superconductors. For instance, CeCoIn_5 [65, 115] and CeRhIn_5 [16, 116] have the highest T_c of Ce-based heavy fermion materials, either at ambient or applied pressure, which is generally ascribed to the quasi two-dimensional nature of the spin fluctuations. Further analogous compounds with the formula $\mathrm{Ce}_n\mathrm{M}_m\mathrm{In}_{3n+2m}$ have also been synthesized, such as $\mathrm{Ce}_3\mathrm{PdIn}_{11}$ [117, 118], $\mathrm{Ce}_2\mathrm{PdIn}_8$ [77], and $\mathrm{CePt}_2\mathrm{In}_7$ [58, 59].

$CePd_2Si_2$ is also a heavy Fermion compound with an enhanced specific heat coefficient $\gamma \simeq 110$ mJ/(mol K^2) [42]. $CePd_2Si_2$ enters an antiferromagnetic state below $T_N = 10$ K [43], very close to its Kondo temperature $T_K = 10$ K [119]. The ordered moment is just $0.62\mu_B$, with $\mathbf{q} = (\frac{1}{2}, \frac{1}{2}, 0)$, as confirmed by neutron scattering measurements at ambient pressure [43]. With increasing pressure, T_N monotonically decreases and drops below 1 K at around 2.6 GPa [10], while neutron diffraction measurements confirm a decrease of the ordered moment [120]. A linear extrapolation of the $T_N - p$ curve to zero temperature gives a critical pressure of $p_c = 2.8$ GPa. Slightly below p_c, superconductivity emerges, which reaches a maximum transition temperature of $T_c = 0.5$ K at p_c [10]. Around p_c, the electrical resistivity shows non-Fermi liquid behavior up to temperatures greater than 20 K, with an almost linear relation $\Delta\rho \propto T^{1.2}$. The magnetic transition at p_c is generally believed to be second-order, while a first-order transition can not be entirely excluded due to the limitation of pressure [120]. The angular dependent de Haas-van Alphen (dHvA) effect measurements [121] are consistent with band structure calculations with the assumption of itinerant $4f$ electrons in the antiferromagnetic state, suggesting there is an itinerant SDW type quantum critical point at p_c in $CePd_2Si_2$.

The isoelectronic compound $CeNi_2Ge_2$ does not magnetically order at ambient pressure [45]. However, C/T exhibits a logarithmic divergence at low temperatures with a large Sommerfeld coefficient $\gamma \simeq 350$ mJ/(mol K^2) [45, 122]. The temperature dependence of the resistivity also shows non-Fermi liquid behavior, with a reported exponent n between 1.1 and 1.5 [46, 122], where higher quality samples generally have a smaller n. It has been proposed that $CeNi_2Ge_2$ is located near a three dimensional antiferromagnetic QCP [123], and the system can be driven to a QCP by doping the Ni site with about 6.5% Pd [124, 125]. Evidence for a superconducting transition also appears below 0.2 K in resistivity measurements, although zero-resistance has not been reached, and NQR measurements were reported to show a slight decrease in $1/T_1T$, probably caused by this filamentary superconductivity [126]. No bulk superconductivity is reported so far and the existence of superconductivity still requires further confirmation. $CePd_2Si_2$ could be considered to correspond to $CeNi_2Ge_2$ at negative pressure, while $CeNi_2Ge_2$ is situated very close to a magnetic instability at ambient pressure. An interesting feature of $CeNi_2Ge_2$ is the occurrence of a second superconducting region under pressure, ranging from 1.5 to 6.5 GPa [46]. The phase diagram (Fig. 7) encompassing both $CeNi_2Ge_2$ and $CePd_2Si_2$ is reminiscent of the phase diagram of $CeCu_2(Si, Ge)_2$ [14] discussed in the next section.

Superconductivity near a possible first-order magnetic quantum phase transition

$CeRh_2Si_2$ is another heavy fermion compound with the same tetragonal $ThCr_2Si_2$-type crystal structure as $CeCu_2Si_2$. $CeRh_2Si_2$ undergoes an antiferromagnetic transition at $T_{N1} = 36$ K to a state AF1 with propagation vector $\mathbf{q_1} = (\frac{1}{2}, \frac{1}{2}, 0)$, before entering a second antiferromagnetic state (AF2) at $T_{N2} = 25$ K via a first-order transition with an additional propagation vector $\mathbf{q_2} = (\frac{1}{2}, \frac{1}{2}, \frac{1}{2})$ [127, 128]. As shown in Fig. 8 [49], both AF1 and AF2 can be completely suppressed by pressure, at $p_c \simeq 1.06$ GPa and $p_c' \simeq 0.6$ GPa respectively. Unconventional superconductivity is observed around p_c with a maximum $T_c \simeq 0.4$ K [49, 129].

The dHvA measurements under pressure indicate that

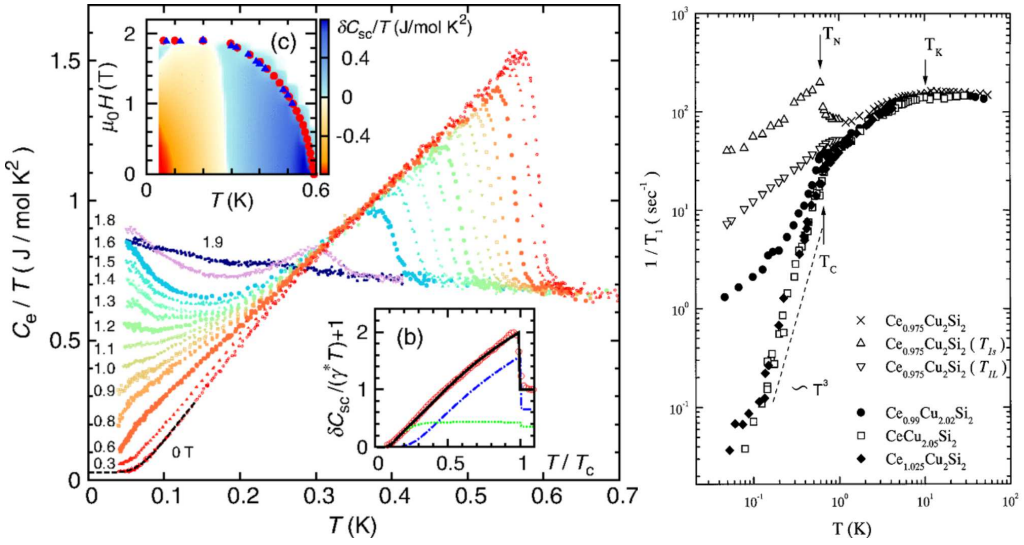

FIG. 6: Specific heat (left) and NQR (right) measurements of superconducting $CeCu_2Si_2$ to low temperatures. The insets show the temperature-field phase diagram and the fitting of the data with a two gap, nodeless model. Adapted with permission from Ref. [108], copyright 2014 the American Physical Society and Ref. [105], copyright 1999 the American Physical Society.

the Fermi surface topology remains unchanged below p_c [130]. Some of the branches observed at low pressure are consistent with the band structure calculations of $LaRh_2Si_2$, indicating there are localized $4f$ electrons, which do not contribute to the volume of the Fermi surface. Note that some branches either appear or disappear at 0.5 GPa, due to the change of magnetic structure inside the antiferromagnetic state. When the pressure is increased through p_c, the topology of the Fermi surface undergoes a sudden change, suggesting that the localized $4f$ electrons may become itinerant. However, thermal expansion measurements show a clear discontinuity in the cell volume, which suggests that the transition from antiferromagnetism to paramagnetism at p_c is probably first-order[131]. Although the A coefficient and residual resistivity ρ_0 reach a maximum around p_c, a T^2 dependence of the resistivity holds across the whole pressure range, in contrast to the non-Fermi liquid behavior generally observed around a QCP [49]. The value of γ only increases to 80 mJ/(mol K^2) at p_c before decreasing smoothly above p_c [47]. This corresponds to only a moderate enhancement of the effective mass, indicating that a significant enhancement of critical fluctuations around p_c is probably avoided in $CeRh_2Si_2$, due to the first-order nature of the AFM to paramagnetic transition.

Measurements of $CeRh_2Si_2$ under pressure can be compared to those in magnetic fields, using techniques such as torque, magnetostriction and transport measurements [132]. The field-temperature phase diagram demonstrates that both AF1 and AF2 are gradually suppressed with increasing magnetic field and merge into a tetracritical point T_{TCP}, with a third phase AF3 emerging in a narrow field range between 25.7 and 26 T. Above the critical magnetic field $H_c \sim 26.0$ T, the system enters the polarized paramagnetic state. The resistivity coefficient A and residual resistivity show similar behavior at H_c as that under pressure, while the abrupt change in the resistivity at 26 T suggests a probable Fermi surface reconstruction at H_c. Whether this reconstruction corresponds to a Kondo-breakdown QCP or first-order transition remains unresolved. It has also been suggested that $CeRh_2Si_2$ could be pushed to a valence critical point by applying a magnetic field at pressures greater than p_c, which may explain recent thermoelectric power (TEP) measurements [130].

Noncentrosymmetric heavy fermion superconductors

Another widely studied class of heavy fermion superconductors are those with noncentrosymmetric crystal structures. One consequence of the lack of inversion symmetry is that in the presence of antisymmetric spin orbit coupling, the superconducting state is neither purely singlet or triplet, but a mixture of the two [96]. $CePt_3Si$ is one such compound which orders antiferromagnetically at $T_N = 2.2$ K and becomes superconducting at $T_c = 0.75$ K [79]. Strong hybridization between the $4f$ and conduction electrons is evidenced by the enhanced value of $\gamma = 390$ mJ/(mol K^2) and a small ordered moment of 0.16 μ_B/Ce [133], which is significantly reduced below the value expected from the crystalline-electric-field (CEF) scheme [134]. Upon applying pressure, T_N decreases and is quickly suppressed around $0.5 - 0.6$ GPa (Fig. 9(a)) [81, 135]. However, unlike many other heavy fermion superconductors which show a superconducting

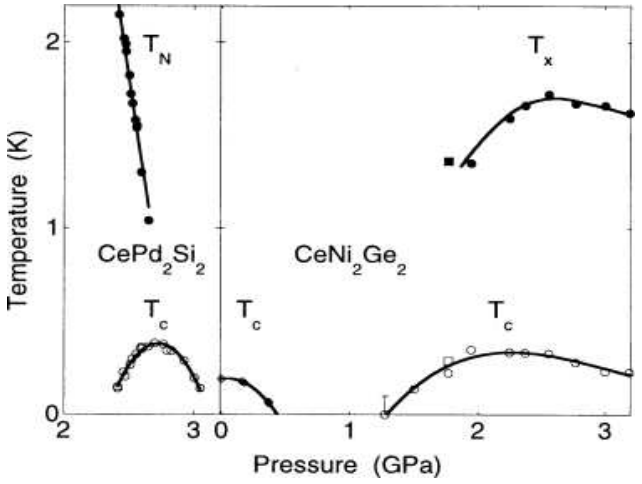

FIG. 7: Temperature-pressure phase diagram of $CePd_2Si_2$ (left) and $CeNi_2Ge_2$ (right). The pressure dependence of the ordering temperature T_N and superconducting transition T_c are shown. Reprinted with permission from Ref. [46]. Copyright 2000 the Institute of Physics.

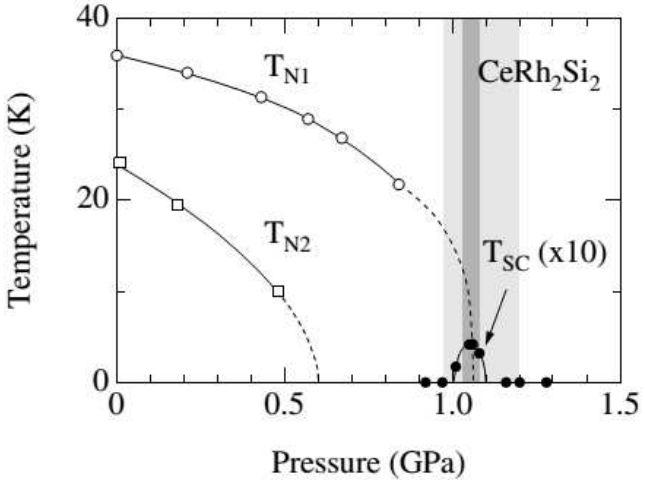

FIG. 8: Temperature-pressure phase diagram of $CeRh_2Si_2$. The ordering temperatures T_{N1} and T_{N2} are suppressed by pressure, with superconductivity being observed near the disappearance of T_{N1}. Reprinted with permission from Ref. [49]. Copyright 2002 the Institute of Physics.

dome with a maximum of T_c in close proximity to the suppression of magnetic order, the T_c of $CePt_3Si$ is largest at ambient pressure and decreases upon increasing the pressure before disappearing around 1.5 GPa. These results indicate a lack of competition between the superconductivity and magnetism in $CePt_3Si$. This is further supported by μSR measurements [136], which indicate a microscopic coexistence between the phases. In addition, ac heat capacity measurements under pressure [135], show no increase in the heat capacity jump at T_c ($\Delta C_{ac}/C_{ac}(T_c)$) when T_N is suppressed by pressure.

A larger family of noncentrosymmetric heavy fermions are $CeTX_3$ (T = transition metal, X = Si or Ge), which crystallize in the tetragonal $BaNiSn_3$ structure with space group $I4mm$. Some of these compounds such as $CeRhGe_3$, $CeIrGe_3$ and $CePtSi_3$ behave as localized antiferromagnets [86, 137, 138]. Of these, $CeIrGe_3$ displays superconductivity at high pressures, greater than 20 GPa [139], while the other two do not show any evidence of superconductivity up to at least 8 GPa [140, 141]. Other isostructural compounds such as $CeCoSi_3$ and $CeRuSi_3$ are non-magnetic intermediate valence compounds [140, 142] where the local moments are entirely quenched and have large values of T_K. The main focus of interest have been from compounds in between these two extremes, namely $CeRhSi_3$, $CeIrSi_3$ and $CeCoGe_3$. Both $CeRhSi_3$ and $CeIrSi_3$ order antiferromagnetically at $T_N = 1.6$ K and 5 K respectively [86, 87]. The magnetic order of both compounds is of the incommensurate spin density wave type [88, 143], with the magnetic moments orientated in the ab plane and dHvA measurements [144–146] show significant differences to the respective La based analogues, indicating the $4f$ electrons are itinerant. Furthermore, upon applying pressure up to nearly 3 GPa, no drastic change in the Fermi surface of $CeRhSi_3$ was observed and the effective mass steadily decreases with pressure. The temperature-pressure phase diagrams are similar to many other heavy fermion superconductors. While T_N of $CeRhSi_3$ [87, 147] initially slightly increases with applied pressure, it is subsequently suppressed to zero temperature around $p_c = 2.36$ GPa, while a superconducting dome emerges for pressures greater than 1.2 GPa, with T_c reaching a maximum slightly above p_c [90]. Evidence for the presence of a QCP at p_c was inferred from μSR measurements, where T_N and the ordered moment of $CeRhSi_3$ were both reported to be suppressed to zero at a second-order transition at p_c [89]. However, in this region no increase of the A coefficient or residual resistivity is observed, indicating there is little enhancement of spin fluctuations [148]. For $CeIrSi_3$ [92] (Fig. 9(b)), T_N continuously decreases with increasing pressure and superconductivity is observed above 1.8 GPa, with a maximum T_c of around 1.6 K at 2.5 GPa, which is approximately where T_N intersects the superconducting dome.

Different behavior is observed for $CeCoGe_3$ [82, 149] which has a higher ordering temperature of $T_N = 21$ K. At ambient pressure the $4f$ electrons are localized [150, 151] and the magnetic structure is commensurate, consisting of moments ordered along the c axis [83, 152, 153]. The temperature-pressure phase diagram is more complex, with multiple pressure induced magnetic phases and T_N undergoes a series of step-like decreases [154, 155]. At around $p_c = 5.5$ GPa, magnetism is suppressed while a broad superconducting dome is observed [84, 155] from 4.3 GPa, to at least 7.1 GPa. Therefore the properties of the $CeTX_3$ have generally been considered to be

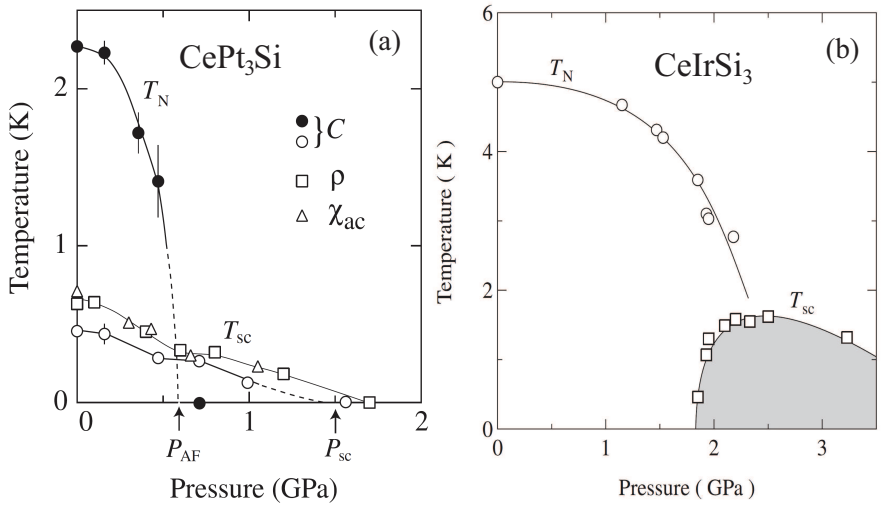

FIG. 9: Temperature-pressure phase diagrams of noncentrosymmetric (a) $CePt_3Si$ and (b) $CeIrSi_3$. Adapted with permission from Ref. [135], copyright 2005 the Physical Society of Japan and Ref. [92], copyright 2006 the Physical Society of Japan respectively.

consistent with the Doniach phase diagram [140], where the system can be tuned from localized magnetism with weak hybridization to intermediate valence behavior with strong hybridization by either elemental substitution or pressure. The effect of chemical pressure may not be sufficient to explain the behavior of all $CeTX_3$ compounds and in particular, for different transition metals T, other changes to the electronic properties may need to be taken into account.

In both the crystal structures of $CePt_3Si$ and $CeTX_3$, inversion symmetry is absent due to the lack of a mirror plane along the c direction. This gives rise to a Rashba type antisymmetric spin-orbit coupling which in general should lead to mixed parity pairing. Indeed there is evidence for unconventional superconductivity in both $CePt_3Si$ [156, 157] and $CeIrSi_3$ [158] from measurements of the superconducting gap structure, which indicate the presence of line nodes in the gap. A particular prediction for the effects of antisymmetric spin-orbit coupling for these crystal structures is an anisotropic spin susceptibility below T_c, which is expected to remain unchanged from the normal state value for fields along the c axis, while reaching half the normal state value for fields in the ab plane [159]. This may be probed either by measuring the NMR Knight shift or the anisotropy of the upper critical field H_{c2}. In the case of the $CeTX_3$ superconductors, H_{c2} is highly anisotropic [85, 90, 93], and in $CeRhSi_3$ it reaches around 30 T for fields along the c axis, but just 7 T in the ab plane, which is consistent with the effects of antisymmetric spin-orbit coupling. In addition, the Knight shift of $CeIrSi_3$ [160] is also qualitatively consistent, although the reduction below T_c reaches just 90% of the normal state value, unlike the 50% predicted by the simple model. On the other hand, the H_{c2} of $CePt_3Si$ only shows a small anisotropy [161] and the Knight shift appears constant below T_c in all directions [161], which remains difficult to account for within this scenario.

SUPERCONDUCTIVITY NEAR A CHARGE INSTABILITY

As described in the preceding section, superconductivity in Ce-based heavy fermion metals usually appears while suppressing the AFM order by applying pressure, showing a maximum T_c near the QCP. In this case, it is generally believed that superconducting electrons are paired through critical spin fluctuations. However, the first heavy fermion superconductor $CeCu_2Si_2$, and its sister compounds $CeCu_2Ge_2$ exhibit highly unusual behavior under pressure, with superconductivity extending to very high pressure [162, 163] and a large enhancement of T_c far away from the AFM QCP which is located at ambient pressure for $CeCu_2Si_2$ and $p_{c1} \simeq 11.5$ GPa for $CeCu_2Ge_2$ respectively. Recently, similar phenomena were also shown to occur in $CeAu_2Si_2$ under pressure, where $p_{c1} \simeq 22.5$ GPa [57]. These findings remain a puzzle and challenge the general view that heavy fermion superconductivity only arises via spin fluctuation mediated pairing.

Several theoretical scenarios have been proposed to account for the anomalous properties in $CeCu_2Si_2$ and $CeCu_2Ge_2$. For instance, Thomas *et al* attributed the enhancement of T_c to pressure-induced topological changes of the renormalized heavy bands [164]. Onishi and Miyake studied a generalized Anderson lattice model and found that the local Coulomb repulsion U_{fc} between the

f and the conduction electrons can lead to a valence transition and proposed that superconductivity in $CeCu_2Si_2$ and $CeCu_2Ge_2$ under pressure is mediated by valence fluctuations [38]. A three dimensional periodic Anderson model was also investigated by Ikeda using third-order perturbation theory [165]. It was argued that the dominant interaction is the on-site repulsion U between f electrons and as a result it is difficult to realize superconductivity arising from U_{cf} rather than from U. Instead, he suggested that the T_c enhancement arises from a dramatic change of the Fermi surface topology or a large momentum-independent mass enhancement.

Further progress towards understanding the behavior of $CeCu_2Si_2$ and $CeCu_2Ge_2$ came from the discovery that the superconductivity in the phase diagram comes from the merger of two different superconducting domes [14, 166, 167]. In $CeCu_2Si_2$, the partial substitution of Ge for Si has two main effects [168]. Firstly, the crystal lattice is expanded and therefore magnetic order is stabilized. Secondly, such a substitution introduces additional disorder and reduces the mean free path, which may suppress superconductivity. Upon pressurizing $CeCu_2(Si_{1-x}Ge_x)_2$, the system corresponds to the pure compound $CeCu_2Si_2$ but with enhanced scattering due to disorder. In fact, it was found that T_N for samples with various Ge-content overlap well after taking into account of the shift of the chemical pressure (Fig. 10), suggesting that the magnetic order is robust against disorder and T_N is primarily determined by the lattice parameters. On the other hand, superconductivity in pressurized $CeCu_2(Si_{1-x}Ge_x)_2$ is strongly affected by the substitution of Ge.

In Fig. 10 [167], the $T-p$ phase diagram of $CeCu_2(Si_{1-x}Ge_x)_2$ is displayed where the zero of the pressure axis corresponds to the AFM QCP at $p_{c1}(x)$ for each Ge-concentration. It is noted that both $CeCu_2Si_2$ and $CeCu_2Ge_2$ display a similar phase diagram, showing a continuous superconducting regime over a wide pressure range [162, 163]. By partially substituting Si with Ge ($x = 0.1$), T_c is lowered and the superconducting regime is separated into two disconnected superconducting domes, one sitting near an AFM QCP and the other one taking place at higher pressure with a maximum T_c, near to a possible valence critical end point [14, 167]. Upon further increasing the Ge-content, no superconductivity is observed under pressure. These findings at low pressures demonstrate that $CeCu_2Si_2$ resembles several other Ce-based heavy fermion systems, supporting the common feature of magnetically mediated superconductivity in heavy fermion superconductors [10]. In contrast to many other systems, a new superconducting state emerges at elevated pressures in $CeCu_2Si_2$ and some other isotructural compounds, which has been taken to be the first example of valence-fluctuation mediated superconductivity and is the focus of the rest in this section. Recent measurements show that the upper critical field

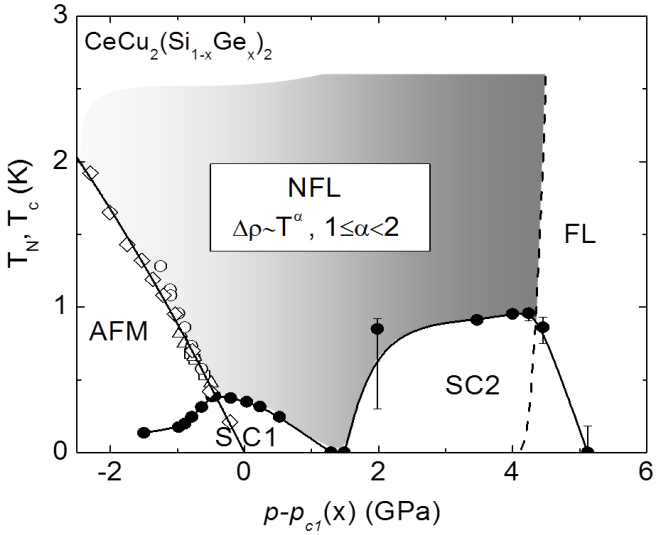

FIG. 10: Temperature-pressure phase diagram of $CeCu_2(Si_{1-x}Ge_x)_2$, showing two superconducting domes under pressure, where $p_{c1}(x)$ is the critical pressure at the AFM QCP for a given Ge doping x. The ordering temperature T_N is shown by the diamonds ($x = 0.25$), open circles ($x = 0.1$), triangles ($x = 0.05$) and squares ($x = 0.01$), while the superconducting transition T_c is shown by the closed circles ($x = 0.1$). Adapted with permission from Ref. [167]. Copyright 2006 the American Physical Society.

[107] and the electronic specific heat [108] of $CeCu_2Si_2$ under pressure follow two distinct scaling behaviors, supporting the scenario of different order parameters in the two superconducting regimes.

In the high-pressure region, the superconducting temperature T_c of $CeCu_2(Si_{1-x}Ge_x)_2$ reaches a maximum value near a second critical point p_{c2} which is associated with a possible first-order valence transition of the Ce ions [14, 167]. As shown in Fig. 11 [167], a few pronounced features are observed near p_{c2}, (1) a linear temperature dependence of the electrical resistivity above T_c, (2) a drop of the electronic scattering as reflected in the resistivity coefficient A and (3) a pronounced maximum of the residual resistivity. Furthermore, a maximum is also observed near p_{c2} in the Sommerfeld coefficient $\gamma(p)$ [41]. All these experimental facts are consistent with theoretical predictions based on a generalized periodic Anderson model as described in Section II and support the proposal that superconductivity in the high-pressure regime is attributed to valence fluctuations. However, there is no direct experimental evidence showing a pressure-induced valence transition in $CeCu_2Si_2$ and $CeCu_2Ge_2$. For $CeCu_2Ge_2$, measurements of angle dispersive X-ray diffraction reveal a weak drop of the unit cell volume at a pressure of $p_{c2} \simeq 15$ GPa at 10 K, which suggests a transition in the Ce valence [169]. However, this anomaly needs be confirmed by further experiments. Recent x-ray absorption spectroscopy mea-

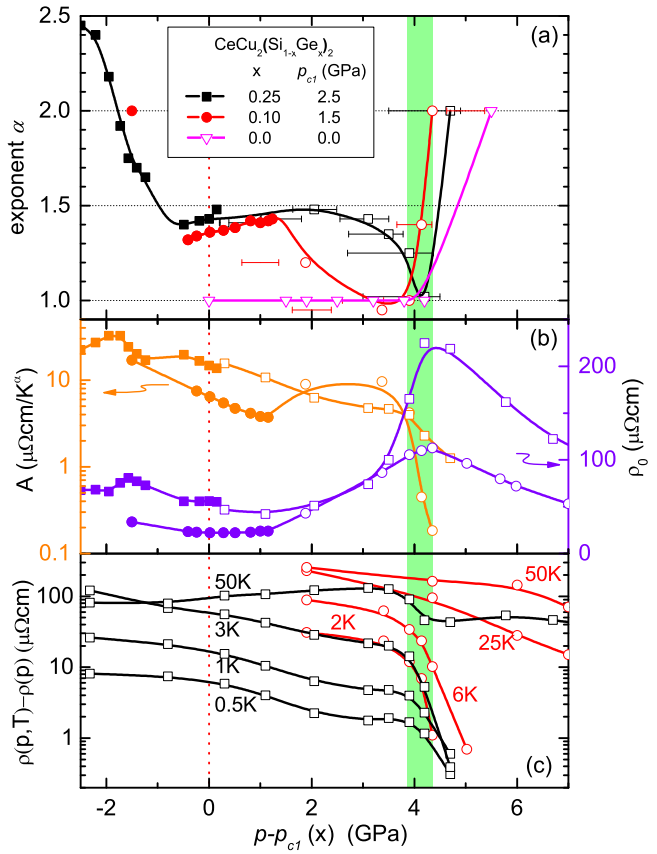

FIG. 11: Pressure dependence of (a) resistivity exponent α, (b) A coefficient and residual resistivity ρ_0 and (c) resistivity isotherms $\Delta\rho_T(p)$ for $CeCu_2(Si_{1-x}Ge_x)_2$ with $x = 0, 0.1$ and 0.25. Adapted with permission from Ref. [167]. Copyright 2006 the American Physical Society.

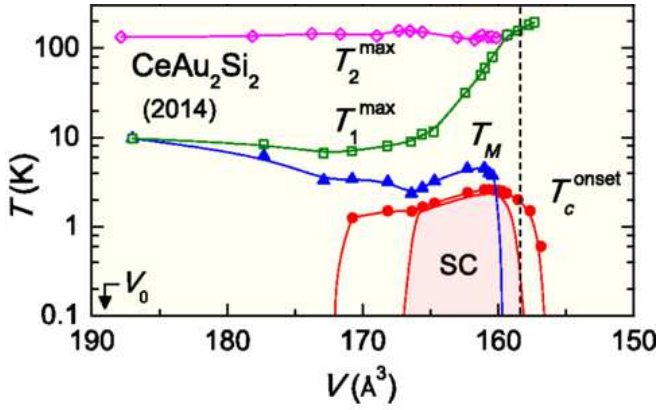

FIG. 12: Temperature-volume phase diagram of $CeAu_2Si_2$, where T_1^{max} and T_2^{max} correspond to maxima in the resistivity, and T_M and T_c correspond to the magnetic ordering and superconducting transition temperatures respectively. Adapted with permission from Ref. [57]. Copyright 2014 the American Physical Society.

surements demonstrate that the Ce valence in $CeCu_2Si_2$ changes continuously with increasing pressure at low temperatures [170, 171]. This suggests that if there is a first-order valence transition, the end point must lie at low temperatures. Furthermore, in $CeCu_2(Si_{1-x}Ge_x)_2$, a sharp drop is observed in the isothermal pressure dependence of the electrical resistivity near p_{c2}, which becomes broad with increasing temperature and vanishes at around 10 K for $x = 0.1$ and around 20 K for $x = 0.25$ [167]. A more recent analysis of the isothermal resistivity of $CeCu_2Si_2$ suggests that the valence transition reaches a critical end point around $p_{c2} = 4.5$ GPa, at a negative temperature [172]. These transport measurements indicate that there may be a valence transition at very low temperatures but to date it has been challenging to detect this in x-ray based experiments.

Recently, pressure-induced superconductivity was also found in antiferromagnetic $CeAu_2Si_2$, another compound isostructural and isoelectronic to $CeCu_2Si_2$ [57]. Unlike $CeCu_2Si_2$, the phase diagram in Fig. 12 shows that superconductivity and antiferromagnetism coexist over a broad pressure range in $CeAu_2Si_2$, showing a parallel increase of T_c and T_M in the pressure range of 16.7 GPa $< p <$ 22.3 GPa, where T_M possibly corresponds to a magnetic transition. This behavior again challenges the widely accepted proposal of spin fluctuation mediated superconductivity in heavy fermion compounds and the relationship between superconductivity and magnetism in the high pressure region remains unclear. It is important to find out whether the anomaly observed above T_c is a continuous evolution of the antiferromagnetic transition observed at low pressures. We note that T_N of $CeAu_2Si_2$ shows a minimum around $p \simeq 16$ GPa, at which one can not exclude the possible suppression of the ambient-pressure antiferromagnetic transition.

It has also been proposed that fluctuations associated with orbital transitions can arise in heavy fermion systems [173]. Using dynamical mean-field theory (DMFT), it was predicted that in $CeCu_2Si_2$ under pressure, there is a transition from the Ce $4f$ electron predominantly occupying the atomic CEF ground state, to it mainly occupying one of the excited states [174]. It was further suggested that the fluctuations corresponding to this transition may lead to the superconducting dome at higher pressures. Orbital transitions were also predicted to occur under pressure in both $CeAu_2Si_2$ and $CeCu_2Ge_2$ [57], and it was suggested that the different temperature-pressure phase diagram of $CeAu_2Si_2$ arises due to different occupations of the CEF levels by the $4f$ electron. However, evidence for this scenario has not yet been found experimentally and there appear to be discrepancies between measurements such as nonresonant inelastic x-ray scattering (NIXS) and the predictions from DMFT [175]. As a result, further experimental and theoretical efforts are necessary in order to elucidate the role of var-

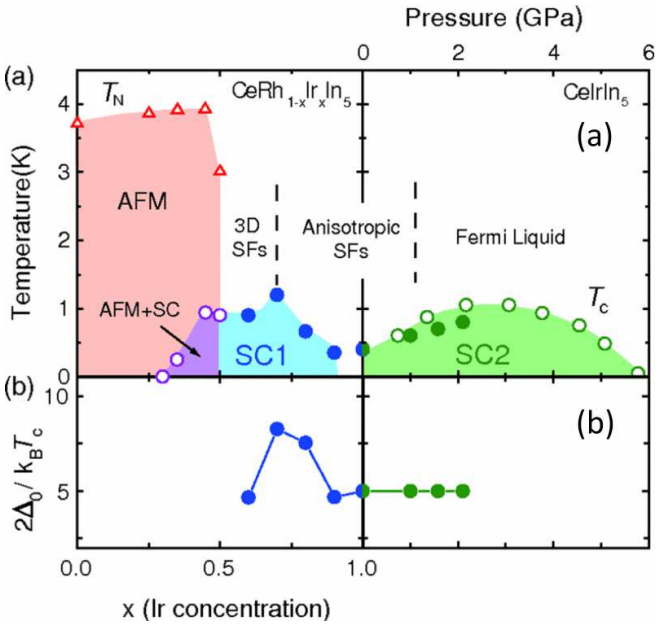

FIG. 13: (a) Combined phase diagram of both $CeRh_{1-x}Ir_xIn_5$ and $CeIrIn_5$ as a function of Ir concentration x and pressure, showing the presence of magnetism and two superconducting domes. (b) The magnitude of the superconducting gap $2\Delta/k_BT_c$ across the superconducting regions, as a function of x. Adapted with permission from Ref. [176]. Copyright 2006 the American Physical Society.

ious degrees of freedom in the superconductivity of these compounds.

Besides $CeCu_2Si_2$ and similar compounds, the presence of two-superconducting domes has also been suggested for Ce(Rh,Ir)In_5 [176, 177] and the PuTIn$_5$ compounds [178]. In $CeIrIn_5$, ^{115}In-NQR experiments demonstrate that the antiferromagnetic fluctuations are strongly suppressed with increasing pressure, but T_c increases, reaching a maximum value of about 1 K at around 3 GPa [179]. On the other hand, substituting Ir with Rh gives rise to antiferromagnetic order and enhances T_c [180], with coexistence of superconductivity and magnetism in $CeRh_{1-x}Ir_xIn_5$ for $0.35 < x < 0.5$ [176]. These results suggest that much like $CeCu_2(Si_{1-x}Ge_x)_2$ under pressure [14], two distinct superconducting states may exist in Ce(Rh,Ir)In_5 in the lattice density-temperature phase diagram, as shown in Fig. 13 [176]. Here $CeIrIn_5$ was assumed to be located in the second superconducting dome which had been taken to be close to a charge (or valence) instability [176, 179]. However, our recent studies of substituting Hg and Sn on the In sites, and Pt on the Ir sites indicate that $CeIrIn_5$ is very much close to an AFM QCP, suggesting that spin fluctuations play a critical role in the formation of superconductivity [181]. Furthermore, although there is a change in the orbital anisotropy of the ground-state wave function at lower values of x in $CeRh_{1-x}Ir_xIn_5$, a significant difference is not seen between $x = 0.75$ and $x = 1$, suggesting the lack of an orbital transition when crossing between the two superconducting domes [182]. In the PuTIn$_5$ compounds, it was proposed that $PuCoIn_5$ is in the antiferromagnetic regime, while $PuRhIn_5$ and $PuCoGa_5$ are located in the second superconducting dome [178]. Recently, measurements of resonant ultrasound spectroscopy provide evidence for a softening of the bulk modulus at temperatures above T_c in $PuCoGa_5$, which is characteristic of valence instabilities [178]. This suggests that valence fluctuations may play a crucial role in the unusually high T_c ($\simeq 18.5$ K) of $PuCoGa_5$. Since a similar enhancement of T_c is also observed in $CeCu_2(Si_{1-x}Ge_x)_2$ under pressure, critical valence fluctuations may favor superconductivity at higher temperatures. However, further experiments are needed to confirm the existence of this pairing mechanism in these compounds.

A pressure-induced volume collapse transition, which is usually associated with the depopulation of localized f electrons, has been observed in a number of rare earth elements and compounds. For examples, a pronounced volume collapse transition was shown to exist in the rare earth elements Ce, Pr and Gd under pressure and at room temperature [183]. Similar isostructural electronic transitions were also observed in several intermetallic compounds, such as rare earth monochalcogenides [184] and $YbInCu_4$ [185]. In $YbInCu_4$, the valence transition is suppressed by applying pressure, and a magnetic-like transition develops in the critical pressure regime [186, 187]. Recently, evidence for a pronounced anomaly in the valence under pressure was also found in $Yb_2Ni_{12}As_7$ at around 1 GPa [188]. However, superconductivity has not yet been observed in most of these compounds showing a pronounced valence transition and the conditions which favor superconductivity mediated via the valence-fluctuation mechanism are unclear. In $CeCu_2Si_2$ and similar compounds, we note that there is a weak first-order valence transition with a low-lying critical end point [167, 170] and it may be that these conditions are necessary for such a superconducting state to form.

Upon tuning a system from the heavy fermion to intermediate valence state by increasing the hybridization strength, various degrees of freedom may play important roles in the critical behavior and/or the development of superconductivity. Whether the spin, charge or orbital ordering of the f electrons undergo a critical instability simultaneously or independently is currently unclear. The above discussion demonstrates that the spin and charge channels are sometimes well separated under pressure, showing multiple quantum phase transitions with distinct critical behaviors. Further experimental and theoretical studies are required to elucidate the superconducting pairing states and to understand the critical behavior associated with the instabilities of the various degrees of freedom in heavy fermion systems.

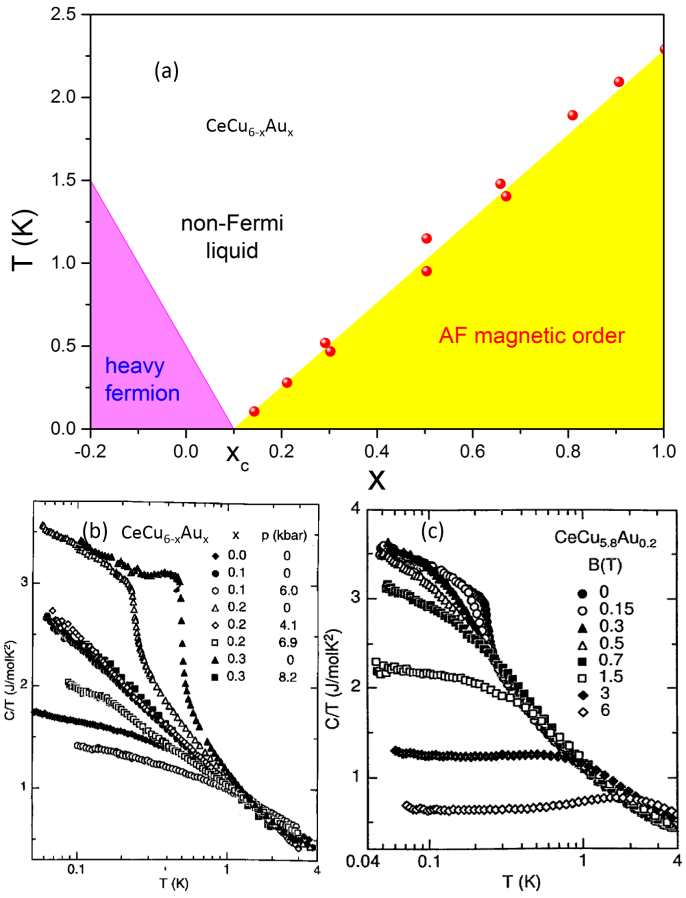

FIG. 14: (a) $T-x$ phase diagram of $CeCu_{6-x}Au_x$ [189]. The negative values of x in the phase diagram correspond to applying a positive pressure. (b) Temperature dependence of the specific heat of $CeCu_{6-x}Au_x$ for different doping levels and pressures. (c) Temperature dependence of the specific heat of $CeCu_{5.8}Au_{0.2}$ in different applied magnetic fields. (b) and (c) are adapted with permission from Ref. [189]. Copyright 1996 the Institute of Physics.

MULTIPLE QUANTUM PHASE TRANSITIONS

The competing phases in heavy fermion compounds typically have a low energy scale, which can be easily tuned by external parameters. Thus, heavy fermion compounds, in particular those based on the elements of Ce and Yb, have been regarded as prototype materials for studying quantum phase transitions. In the preceding sections, we have described superconductivity emerging near magnetic and charge instabilities, which are associated with various degrees of freedom of the f electrons. In this section, we discuss multiple magnetic quantum phase transitions reached upon tuning different parameters, such as pressure, magnetic field and chemical doping, and examine their universal classification.

Several theories of quantum criticality have been proposed for heavy fermions compounds [29–34, 190, 191]. Even though the underlying physics at QCPs is still under debate, the following two scenarios have been widely discussed in the literature. The first scenario is the conventional SDW-type of QCP [11, 29–31], at which the quasiparticles are scattered by critical SDW spin fluctuations, leading to an increased effective mass and a continuous evolution of the Fermi surface across the QCP. It appears that most AFM QCPs where superconductivity is observed are of the SDW-type. At an unconventional local QCP [32, 33], critical fermionic and bosonic degrees of freedom are involved and the Fermi volume undergoes a sudden change as a result of the breakdown of the Kondo effect. As a result, the evolution of the Fermi surface may be used to characterize a QCP and therefore to test theoretical models.

Evidence for various types of critical behavior have been reported in heavy fermion compounds [2, 3] but the universal classification could be complicated by extrinsic factors such as disorder, the measured temperature range and additional symmetry breaking from applied magnetic fields. Furthermore, different scaling behaviors are found in some compounds when different parameters are tuned. The classification of QCPs and the question of whether they show universal behavior remains an open

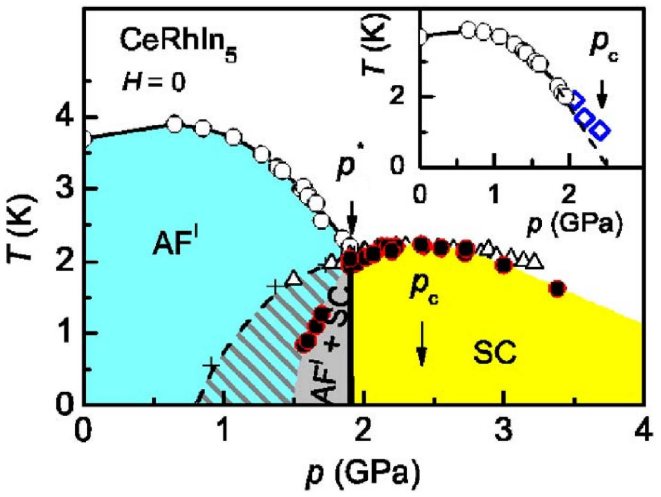

FIG. 15: Temperature-pressure phase diagram of $CeRhIn_5$ Pressure suppresses the magnetism until T_N is equal to T_c at p^*. The inset shows the pressure dependence of T_N in a large enough field, which shows T_N suppressed to zero at p_c. Adapted with permission from Ref. [17]. Copyright 2006 the American Physical Society.

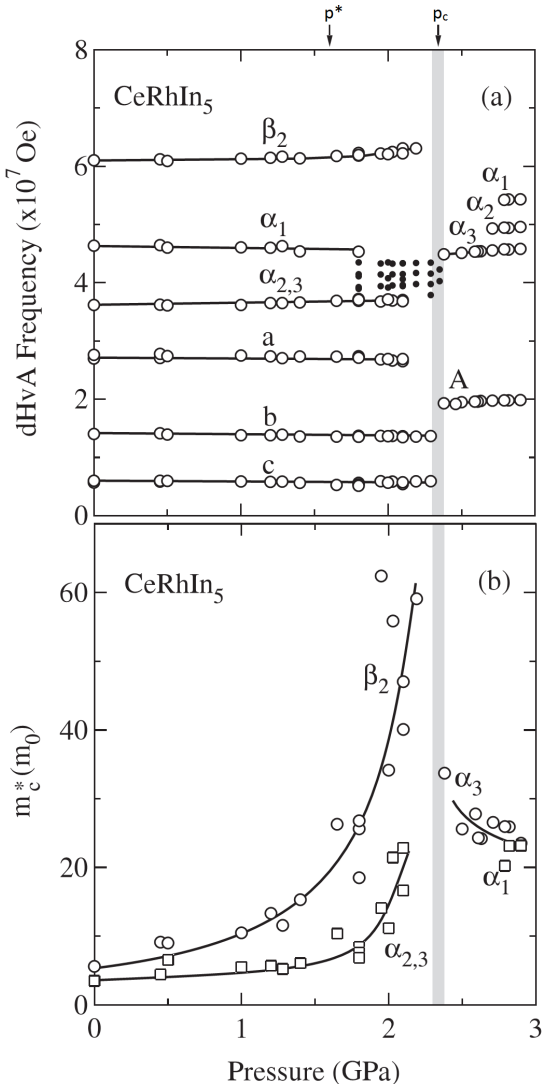

FIG. 16: Pressure dependence of dHvA measurements of $CeRhIn_5$, showing (a) dHvA frequencies and (b) the cyclotron masses. A sudden change of frequencies is seen at p_c, where there is also a sharp upturn of the masses. Adapted with permission from Ref. [192]. Copyright 2005 the Physical Society of Japan

issue. Here we will focus on a few examples where the ground state can be tuned by different parameters.

$CeCu_6$ is an archetypal heavy fermion compound with a large specific heat coefficient $\gamma = 1.6$ J/(mol K^2) [193] and a Kondo temperature T_K of around 6 K [194]. No magnetic order is observed in $CeCu_6$ down to the lowest measured temperatures and the electrical resistivity follows a quadratic temperature dependence, which is a characteristic feature of Fermi liquid behavior. Substituting Au for Cu results in a lattice expansion which reduces J, and as a result long range antiferromagnetic order emerges in $CeCu_{6-x}Au_x$ for $x > x_c \simeq 0.1$ [19], as shown in Fig. 14(a). Around the AFM QCP ($x_c = 0.1$), the system shows pronounced non-Fermi liquid behavior. For instance, the electrical resistivity follows a linear temperature dependence and the specific heat C/T diverges logarithmically with decreasing temperature [189], as shown in Fig. 14(b). The Kondo temperature, as investigated by ultraviolet and x-ray photoemission spectroscopy, shows a step-like change at x_c [195–197], possibly indicating the destruction of heavy quasiparticles. Moreover, neutron scattering experiments also revealed anomalous E/T and H/T scaling of the susceptibility [198], suggesting the development of an unusual kind of localized excitation. These experimental facts support the presence of a unconventional QCP at the critical doping concentration of x_c. Similar critical behavior is also observed when the AFM order of $CeCu_{5.8}Au_{0.2}$ ($T_N \simeq 250$ mK) is suppressed by pressure at $p_c = 4$ GPa [199]. Meanwhile, the application of a small magnetic field ($B_c \simeq 0.4$ T for $H//c$) suppresses the AFM order in $CeCu_{5.8}Au_{0.2}$ and the critical behavior at the field-tuned QCP differs from that induced by pressure or doping [199]. Inelastic neutron scattering measurements demonstrate that the critical fluctuation spectrum of $CeCu_{5.8}Au_{0.2}$ near the critical field B_c is better characterized by the three dimensional SDW scenario rather than the unconventional local scenario found in $CeCu_{5.9}Au_{0.1}$ at zero magnetic field [200]. Moreover, at the field-induced QCP the specific heat and electrical resistivity follow $C/T \propto -T^{0.5}$ (Fig. 14(c)) and $\rho \propto T^{3/2}$ dependencies respectively, which suggest three dimensional SDW-type quantum criticality. These results indicate that different types of critical behavior can be induced by pressure and magnetic field and multiple QCPs may exist in the same compound. Besides $CeCu_{6-x}Au_x$, evidence for QCPs with different behav-

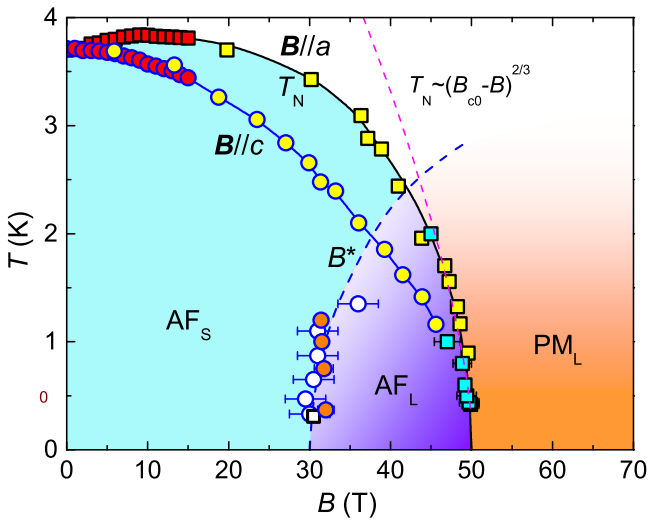

FIG. 17: Temperature - magnetic field phase diagram of $CeRhIn_5$ at ambient pressure. The line B^* separates the antiferromagnetic phases with large (AF_L) and small (AF_S) Fermi surface volumes. Adapted with permission from Ref. [18]. Copyright 2015 the National Academy of Sciences of the United States of America.

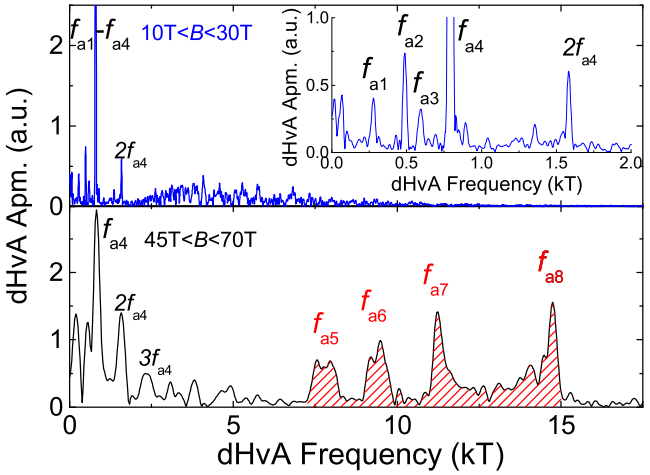

FIG. 18: Fourier spectra of the dHvA oscillations of $CeRhIn_5$ at ambient pressure, over field windows of 10 T $< B <$ 30 T (top) and 45 T $< B <$ 70 T (bottom). In the high field region, four new dHvA frequencies are observed. Adapted with permission from Ref. [18]. Copyright 2015 the National Academy of Sciences of the United States of America.

iors exist for other compounds. For example, there is a growing body of experimental evidence suggesting an unconventional local QCP in $YbRh_2Si_2$ under applied magnetic field [201–203], although alternative theoretical models have also been proposed [190, 204, 205]. On the other hand, chemical pressure via the substitution of Ir or Co leads to the separation of the AFM QCP and Kondo breakdown line [206], and in the case of Ir doping, it was suggested that a spin-liquid-type ground state may emerge. However, we will mainly focus on Ce-based heavy fermion compounds and an extensive discussion of other compounds is beyond the scope of this article.

In order to search further evidence for multiple QCPs and to study their classification, we have recently extended measurements of $CeRhIn_5$ to very high magnetic fields and pressure, which have revealed remarkable new physics. $CeRhIn_5$ belongs to the well-investigated $CeTIn_5$ (T = Co, Rh, Ir) family of compounds. At ambient pressure, $CeRhIn_5$ orders antiferromagnetically below $T_N = 3.8$ K [67], but $CeCoIn_5$ and $CeIrIn_5$ are heavy fermion superconductors [65, 71]. Previous dHvA measurements on La-substituted $CeTIn_5$ samples have shown that the Ce-4f electrons are itinerant in $CeCoIn_5$ and $CeIrIn_5$ but localized in $CeRhIn_5$ [207, 208]. This conclusion is further supported by a comparison of the experimentally derived dHvA frequencies with band structure calculations under the assumption that the 4f electrons are either localized or itinerant[18, 209]. These results demonstrate that in ambient conditions $CeRhIn_5$ possesses a small Fermi surface volume, but in $CeCoIn_5$ the f electrons contribute to the Fermi sea and therefore the volume of the Fermi surface is enlarged. Such an expansion of the Fermi volume may correspond to the delocalization of Ce-4f electrons with increasing the hybridization strength.

The application of hydrostatic pressure suppresses the antiferromagnetic order in $CeRhIn_5$ and induces superconductivity [16, 17], as shown in Fig. 15. Superconductivity and magnetism coexist below $p^* \simeq 1.75$ GPa. In the pressure range $p^* < p < p_c = 2.3$ GPa, magnetism is hidden inside the superconducting state at $B = 0$ and long-range magnetic order is recovered by applying a magnetic field. This allows the tracking of the pressure-induced magnetic QCP at $p_c \simeq 2.3$ GPa[16]. As shown in Fig. 16, a pressure-induced dramatic change of the dHvA frequencies and a divergence of the effective mass are observed in $CeRhIn_5$ at the AFM QCP [207], which have been regarded as experimental evidence to support the unconventional local QCP scenario [6]. On the other hand, the antiferromagnetic order is robust against magnetic field [207], allowing us to study the evolution of the Fermi surface with applied field. This is not possible for $CeCu_{6-x}Au_x$ and $YbRh_2Si_2$ due to the small values of the critical fields. Therefore, $CeRhIn_5$ may be a model system to study multiple QCPs and their relationship to the Fermi surface reconstruction, which motivated us to systematically study the properties of $CeRhIn_5$ under the extreme conditions of high magnetic field and high pressure, using high-field facilities.

Measurements of the ac specific heat and magnetic susceptibility allowed us to map the $B - T$ phase diagram of $CeRhIn_5$ (Fig. 17) [18]. It can be seen that T_N is eventually suppressed with increasing magnetic field for $H//a$ and $H//c$, which converge to the same critical

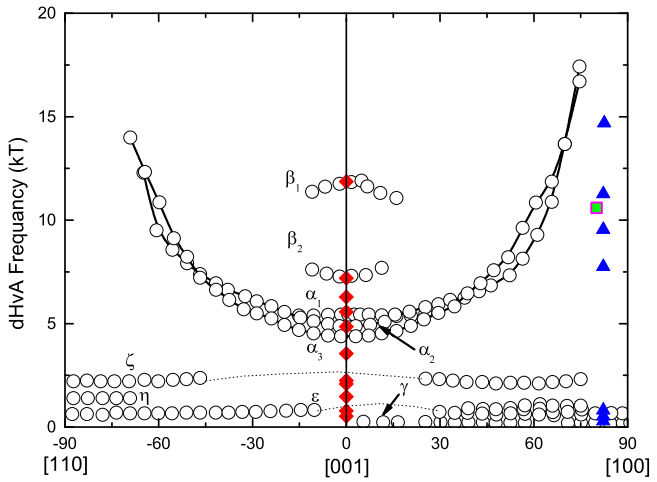

FIG. 19: Comparison of the dHvA frequencies of $CeRhIn_5$ at $B > B^*$ and $CeCoIn_5$ (black open circles). The similarity between the two materials suggests that the $4f$ electrons of $CeRhIn_5$ are delocalized at high magnetic fields. Adapted with permission from Ref. [18]. Copyright 2015 the National Academy of Sciences of the United States of America.

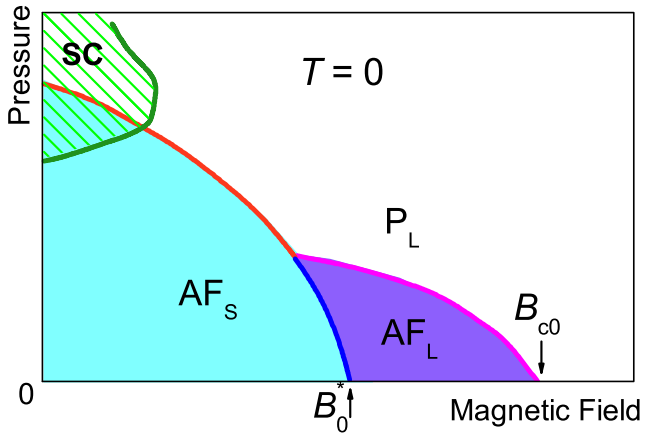

FIG. 20: Schematic pressure-field phase diagram of $CeRhIn_5$ at zero temperature, where different behaviors of the QCPs are seen when pressure and magnetic fields are applied. Adapted with permission from Ref. [18]. Copyright 2015 the National Academy of Sciences of the United States of America.

field at the AFM QCP ($B_{c0} \simeq 50$ T). It is remarkable that the magnetic order is suppressed at nearly the same critical field for the two different field orientations, since this compound possesses a quasi-two dimensional crystal structure. Furthermore, near B_{c0} the behavior follows $T_N \sim (B_{c0} - B)^{2/3}$ $(H//a)$, which indicates three dimensional spin fluctuations.

More interestingly, a field-induced reconstruction of the Fermi surface is observed around $B^* \simeq 30$ T and at temperatures below 2 K [18], which is well inside the AFM state of $CeRhIn_5$ (see Fig. 17). Evidence for a pronounced change of the dHvA frequencies was first found in dHvA measurements up to applied fields of 72 T, using a pulsed magnetic field at Los Alamos National Laboratory, as shown in Fig. 18 [18]. This important observation was later confirmed by measurements of the torque magnetization and Hall resistivity [18], which clearly show a change around $B^* \simeq 30$ T for both $H//c$ and $H//a$. For $B > B^*$, new dHvA frequencies with much larger values are observed, suggesting an expansion of the Fermi volume above B^*. Moreover, we found that the dHvA frequencies of $CeRhIn_5$ in the field range $B > B^*$ are very much compatible with those of $CeCoIn_5$ (see Fig. 19), indicating that the Ce-$4f$ electrons become delocalized at $B > B^*$ [18]. By fabricating a microstructure of $CeRhIn_5$ using the focused ion beam technique, Moll *et al* found hysteresis around $B^* \simeq 30$ T in the in-plane resistivity with the field applied close to the c-axis, where a Fermi surface reconstruction is also observed [210]. They argued that a density wave transition may occur at B^* [210]. However, our recent measurements of the magnetostriction down to 0.6 K using a pulsed magnetic field do not show any feature at $B^* = 30$ T [211], indicating that the transition at B^* is unlikely to be driven by electron-phonon coupling, as would be the case for charge density wave order.

Fig. 20 shows a schematic $p - B$ phase diagram of $CeRhIn_5$ at zero temperature [18]. The pressure-induced AFM QCP is characterized by a dramatic change of the Fermi surface from the AFM state with a small volume (AF_S) to the paramagnetic Fermi surface with a large volume (P_L) upon increasing the pressure. These observations seem to support the scenario of a local QCP [6, 32], with the occurrence of superconductivity near the QCP. On the other hand, upon suppressing the AFM state by increasing the magnetic field, a reconstruction of the Fermi surface occurs at B^*, deep inside the AFM state of $CeRhIn_5$ [18]. The measurements of quantum oscillations and Hall resistivity, together with band structure calculations, indicate there is a possible Kondo breakdown transition at B^*, which leads to a change from a small Fermi surface volume (AF_S) to a large Fermi surface volume (AF_L) [18]. At the magnetic field-induced QCP, the Fermi surface evolves smoothly from the AFM state to the paramagnetic state, indicating it is of the SDW-type. This is also consistent with the critical point being the same for fields along the a- and c-axes. From this phase diagram, one can see that multiple quantum phase transitions can be induced by tuning different parameters in the same compound. Furthermore, two distinct QCPs may exist under magnetic field in $CeRhIn_5$, a Kondo breakdown QCP at B^* and a SDW QCP at B_{c0}. These experimental findings not only provide new perspectives on $CeRhIn_5$, but also suggest that the change of the Fermi surface volume may allow the classification of the different scenarios proposed for QCPs. To test the universality of this behavior, it is important to map the

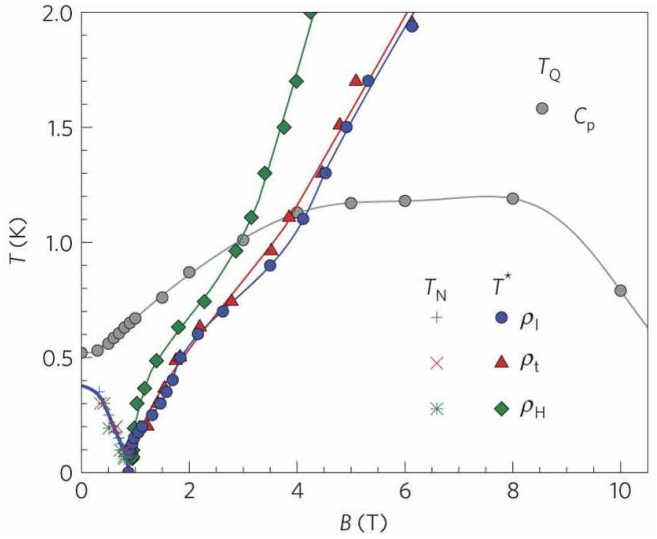

FIG. 21: Temperature-field phase diagram of $Ce_3Pd_{20}Si_6$, which shows the antiferromagnetic ordering temperature T_N, the quadrupolar ordering temperature T_Q and T^*, which characterizes the crossover from localized to itinerant behavior of the $4f$ electrons. Adapted with permission from Ref. [212]. Copyright 2012 the Nature Publishing Group.

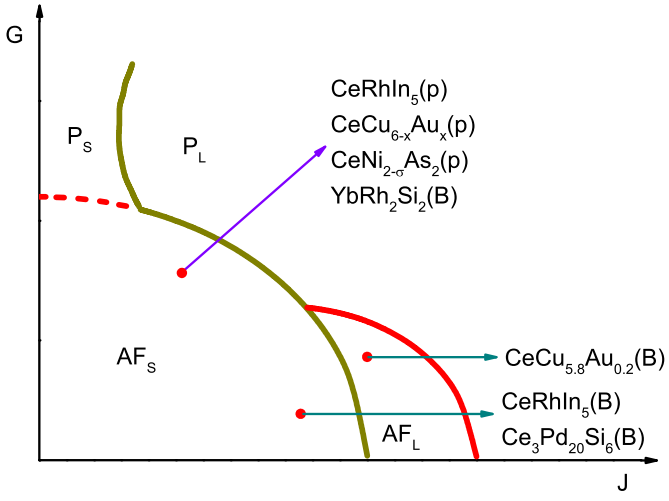

FIG. 22: Global phase diagram for heavy fermion systems [20, 22]. The parameter J is the coupling strength, while G characterizes the degree of frustration. The phases AF_S and AF_L are magnetically ordered with large and small Fermi surface volumes respectively, while P_S and P_L are the respective paramagnetic phases. Schematic trajectories for different materials are displayed based on experimental results obtained via tuning pressure (p) or applied magnetic fields (B).

$B-p$ phase diagram of $CeRhIn_5$ and extend these investigations to other heavy fermion systems, with localized f electrons.

Very recently, differences were also observed between the pressure- and field- tuning of $CeNi_{2-\sigma}As_2(\sigma \simeq 0.28)$ [213], which crystallizes in a $CaBe_2Ge_2$-type structure with $T_N \simeq 5.1$ K. This compound shows semimetallicity with a low charge carrier density and a moderate degree of magnetic frustration. The application of pressure suppresses the AFM transition, with a critical pressure near $p_c = 2.7$ GPa derived from ac specific heat measurements. However, an upturn is observed in the electrical resistivity at temperatures below 2 K in the pressure range 2.02 GPa $< p <$ 3.5 GPa, the origin of which is unknown. At low pressures ($p < p_c$), a step like jump is observed in the Hall resistivity ρ_{xy}, which is explained by a spin-flop transition. The coherence temperature seems to vanish at p_c, for which a scenario of a Kondo destruction QCP was proposed. However, there is still little evidence for either a Fermi surface change or a jump in the charge carrier density at p_c. On the other hand, the antiferromagnetic order is also suppressed by applying a magnetic field of $B_c = 2.8$ T, where the field-induced QCP is assumed to be close to the quantum critical end point of a spin-flop transition.

The caged compound $Ce_3Pd_{20}Si_6$ is another example useful for studying the effects of the dimensionality on quantum criticality [212]. This compound crystallizes in a cubic structure with space group $Fm\bar{3}m$ and carries a huge specific heat coefficient of $\gamma = 8$ J/(mol K^2). As shown in Fig. 21, with decreasing temperature, $Ce_3Pd_{20}Si_6$ undergoes two subsequent phase transitions at 0.53 K and 0.33 K, which correspond to quadrupolar and antiferromagnetic transitions respectively. The quadrupolar transition temperature T_Q first increases with the application of magnetic fields and peaks at 8 T, with $T_Q \simeq 1.2$ K, before decreasing at larger fields. Further increasing the magnetic field will suppress T_Q completely, implying a possible field-induced quantum critical point above 10 T. Inside the quadrupolar phase, the antiferromagnetic transition temperature T_N is suppressed monotonically by applying a field and reaches zero at a critical field around 0.9 T. In an applied field of 1 T, near the critical field, the electrical resistivity shows a linear temperature dependence and the specific heat C/T diverges logarithmically, but upon moving away from the critical field, Fermi liquid behavior is recovered. Moreover, the crossover temperature line $T^*(B)$, where there is a change of the Hall coefficient, merges with the $T_N(B)$ line at this critical field inside the quadrupolar ordered state, similar to the field-induced Kondo breakdown observed in $CeRhIn_5$ [18]. It was suggested that the increased dimensionality of the three dimensional cubic crystal structure of $Ce_3Pd_{20}Si_6$ compared to $YbRh_2Si_2$, means that the magnetic frustration in the global phase diagram is reduced and therefore the two compounds follow different paths.

To summarize this section, we plot a materials-based global phase diagram in Fig. 22. Pressure, magnetic field, doping and lattice dimensionality are possible tuning parameters for quantum criticality in heavy fermion

compounds. From Fig. 22, three typical tuning routes from the AF_S phase to P_L can be considered [20, 21]. Firstly the system can cross directly to the P_L state, which corresponds to a local QCP. Secondly there may be a change of Fermi surface volume in the ordered state as the system goes from AF_S to AF_L, before passing through a SDW QCP. Finally, the system may bridge the AF_S and P_L states by passing through the disordered P_S phase. It can be seen that different scenarios for QCPs predicted in the global phase diagram can be realized either in different materials or in the same material with different tuning parameters. To classify the multiple quantum phase transitions, the evolution of the Fermi surface is an important indicator. Besides the conventional SDW-type QCP and the unconventional local QCP which have been discussed frequently in the literature, the Kondo breakdown transition inside the magnetically ordered state may present another new scenario for quantum criticality, which should be explored. Furthermore, more experimental evidence is needed to elucidate the Kondo breakdown transition, and new materials will help establish the applicability of the global phase diagram.

SUMMARY AND PROSPECTS

In heavy fermions compounds, energy scales associated with the various degrees of freedom are well separated and the effects of strong electronic correlations can be studied without being complicated by other excitations, *e.g.*, lattice dynamics. Moreover, the availability of very clean heavy fermion samples together with clean tuning parameters such as pressure allows us to study the fundamental physics without the influence of disorder. Applications of pressure, magnetic field and doping may enhance the hybridization between f and conduction electrons, which can lead to a delocalization of the f electrons, changing the ground state from antiferromagnetism to a heavy fermion paramagnet. Upon crossing the AFM QCP, unconventional normal and superconducting states emerge. When the hybridization is further increased, the f electrons can hop between different valence states, which may also lead to novel behavior in the vicinity of a valence instability. Therefore, Ce-based heavy fermion compounds are prototype systems for studying unconventional superconductivity and multiple quantum phase transitions, which are induced either by tuning the magnetic state with different parameters or by tuning one parameter through instabilities of different degrees of freedom.

Intensive efforts have recently been devoted to the study of quantum phase transitions. However, the fate of quasiparticles at the QCP and the interplay between superconductivity and quantum criticality remains an open question. The universal classification of QCPs is essential for establishing whether there is a global phase diagram for heavy fermions systems and the discovery of new materials or further characterization of known compounds is necessary to test its applicability. Our recent measurements of the dHvA effect and Hall resistivity of $CeRhIn_5$ suggest that the evolution of the Fermi surface may provide a means for classifying QCPs, where the destruction of the Kondo effect leads to a Fermi surface reconstruction. Nevertheless, besides the Kondo destruction scenario [32, 33], alternative models have been proposed to understand the Fermi surface change at the AFM QCP [190, 204, 205, 214].

The identification of the symmetry of the order parameter is important for understanding the pairing mechanism of a superconductor. However, Ce based heavy fermion superconductors usually have quite a low superconducting transition temperature, typically of the order of 1 K or lower, and in many cases superconductivity requires the application of pressure. These conditions largely restrict the range of experimental techniques which can be applied to characterize the superconducting order parameter. Except for $CeTIn_5$ compounds, the order parameters for most of other heavy fermion superconductors have not been thoroughly investigated and in several cases remain controversial. On the other hand, improvements of the experimental resolution of modern techniques and the availability of low-temperature conditions for a wider range of spectroscopic methods, such as ARPES and STM, may provide powerful tools to directly probe the momentum-dependence of the gap structure below T_c. Furthermore, spectroscopic measurements will also help reveal the development of Kondo screening as a function of temperature or other parameters in the normal state.

Heavy fermion superconductors where the crystal structure lacks inversion symmetry have also attracted considerable interest. The absence of inversion symmetry leads to an antisymmetric spin-orbit coupling (ASOC), allowing the admixture of spin-singlet and spin-triplet components in the superconducting pairing state [96]. This mixed pairing state is prohibited in centrosymmetric superconductors, where the parity of the pairing state is a good quantum number. Evidence for nodal superconductivity but with a coherence peak in the spin lattice relaxation rate was observed in noncentrosymmetric $CePt_3Si$ [79, 161]. For pressure-induced superconductivity in $CeRhSi_3$ [147], a huge upper critical field of around $B_{c2} \sim 30$ T was found for fields along the c axis, with just 7 T in the ab plane [90]. These unusual superconducting properties might be related to the absence of inversion symmetry, but separating the effects of the ASOC from those of magnetism and strong electronic correlations are challenging. Superlattices consisting of layers of superconducting $CeCoIn_5$ separated by spacer layers of $YbCoIn_5$ [215], where inversion symmetry is broken at the interface of the two materials provides a system

where the ASOC can be tuned more controllably and indeed, different behavior of $H_{c2}(T)$ is found when the layer thickness is tuned [216, 217]. It may be the case that weakly correlated noncentrosymmetric superconductors are better suited for determining the effects of inversion symmetry breaking, for instance Li_2Pd_3B and Li_2Pt_3B [218]. A comprehensive review article on superconductivity and spin-orbit coupling in non-centrosymmetric compounds will be available [219].

We would like to thank S. Arsenijević, E. D. Bauer, Y. Chen, D. Graf, N. Hussey, M. Jaime, S. Kirchner, Y. Kohama, H. O. Lee, K. Miyake, T. Park, Q. Si, J. Singleton, F. Steglich, J. D. Thompson, Z. Wang, J. Wosnitza, Y. J. Zhang and J.-X Zhu for useful discussions. This work was supported by Natural Science Foundation of China (grant numbers 11474251, 11374257 and 11174245), the Science Challenge Program of China and the Fundamental Research Funds for the Central Universities.

* Electronic address: xinluphy@zju.edu.cn
† Electronic address: hqyuan@zju.edu.cn

[1] G. R. Stewart, Rev. Mod. Phys. **56**, 755 (1984).
[2] G. R. Stewart, Rev. Mod. Phys. **73**, 797 (2001).
[3] H. v. Löhneysen, A. Rosch, M. Vojta, and P. Wölfle, Rev. Mod. Phys. **79**, 1015 (2007).
[4] C. Pfleiderer, Rev. Mod. Phys. **81**, 1551 (2009).
[5] B. D. White, J. D. Thompson, and M. B. Maple, Physica C **514**, 246 (2015).
[6] Q. Si and F. Steglich, Science **329**, 1161 (2010).
[7] A. C. Hewson, *The Kondo Problem to Heavy Fermions* (Cambridge University Press, Cambridge, 1993), ISBN 978-0521599474.
[8] P. Coleman, *Heavy Fermions:electrons at the edge of magnetism. Handbook of Magnetism and Advanced Magnetic Materials*, vol. 1 (Wiley, New York, 2007).
[9] F. Steglich, J. Aarts, C. D. Bredl, W. Lieke, D. Meschede, W. Franz, and H. Schäfer, Phys. Rev. Lett. **43**, 1892 (1979).
[10] N. D. Mathur, F. M. Grosche, S. R. Julian, I. R. Walker, D. M. Freye, R. K. W. Haselwimmer, and G. G. Lonzarich, Nature **394**, 39 (1998).
[11] P. Monthoux, D. Pines, and G. G. Lonzarich, Nature **450**, 1177 (2007).
[12] M. R. Norman, Science **332**, 196 (2011).
[13] D. J. Scalapino, Rev. Mod. Phys. **84**, 1383 (2012).
[14] H. Q. Yuan, F. M. Grosche, M. Deppe, C. Geibel, G. Sparn, and F. Steglich, Science **302**, 2104 (2003).
[15] D. Wohlleben and J. Röhler, J. Appl. Phys. **55**, 1904 (1984).
[16] T. Park, F. Ronning, H. Q. Yuan, M. B. Salamon, R. Movshovich, J. L. Sarrao, and J. D. Thompson, Nature **440**, 65 (2006).
[17] G. Knebel, D. Aoki, D. Braithwaite, B. Salce, and J. Flouquet, Phys. Rev. B **74**, 020501 (2006).
[18] L. Jiao, Y. Chen, Y. Kohama, D. Graf, E. D. Bauer, J. Singleton, J.-X. Zhu, Z. Weng, G. Pang, T. Shang, et al., Proc. Natl. Acad. Sci. USA **112**, 673 (2015).
[19] O. Stockert and F. Steglich, Annu. Rev. Condens. Matter Phys. **2**, 79 (2011).
[20] Q. Si, Physica B **378-380**, 23 (2006).
[21] Q. Si, physica status solidi (b) **247**, 476 (2010).
[22] P. Coleman and A. H. Nevidomskyy, J. Low. Temp. Phys. **161**, 182 (2010).
[23] S. Doniach, Physica B+C **91**, 231 (1977).
[24] J. Kondo, Prog. Theor. Phys. **32**, 37 (1964).
[25] C. Lacroix, J. Magn. Magn. Mater. **60**, 145 (1986).
[26] M. A. Ruderman and C. Kittel, Phys. Rev. **96**, 99 (1954).
[27] T. Kasuya, Prog. Theor. Phys. **16**, 45 (1956).
[28] K. Yosida, Phys. Rev. **106**, 893 (1957).
[29] J. A. Hertz, Phys. Rev. B **14**, 1165 (1976).
[30] A. J. Millis, Phys. Rev. B **48**, 7183 (1993).
[31] T. Moriya, *Spin Fluctuations in Itinerant Electron Magnetism* (Springer Berlin Heidelberg, 1985).
[32] Q. Si, S. Rabello, K. Ingersent, and J. L. Smith, Nature **413**, 804 (2001).
[33] P. Coleman, C. Pépin, Q. Si, and R. Ramazashvili, J. Phys. Condens. Matter **13**, R723 (2001).
[34] C. Pépin, Phys. Rev. Lett. **98**, 206401 (2007).
[35] P. Gegenwart, Q. Si, and F. Steglich, Nature Physics **4**, 186 (2008).
[36] P. W. Anderson, Phys. Rev. **124**, 41 (1961).
[37] J. R. Schrieffer and P. A. Wolff, Phys. Rev. **149**, 491 (1966).
[38] Y. Onishi and K. Miyake, J. Phys. Soc. Jpn. **69**, 3955 (2000).
[39] S. Watanabe and K. Miyake, J. Phys. Condens. Matter **23**, 094217 (2011).
[40] K. Miyake and H. Maebashi, J. Phys. Soc. Jpn. **71**, 1007 (2002).
[41] A. T. Holmes, D. Jaccard, and K. Miyake, Phys. Rev. B **69**, 024508 (2004).
[42] S. K. Dhar and E. V. Sampathkumaran, Phys. Lett. A **121**, 454 (1987).
[43] B. H. Grier, J. M. Lawrence, V. Murgai, and R. D. Parks, Phys. Rev. B **29**, 2664 (1984).
[44] I. Sheikin, E. Steep, D. Braithwaite, J.-P. Brison, S. Raymond, D. Jaccard, and J. Flouquet, J. Low Temp. Phys. **122**, 591 (2001).
[45] G. Knopp, A. Loidl, R. Caspary, U. Gottwick, C. D. Bredl, H. Spille, F. Steglich, and A. P. Murani, J. Magn. Magn. Mater. **74**, 341 (1988).
[46] F. M. Grosche, P. Agarwal, S. R. Julian, N. J. Wilson, R. K. W. Haselwimmer, S. J. S. Lister, N. D. Mathur, F. V. Carter, S. S. Saxena, and G. G. Lonzarich, J. Phys. Condens. Matter **12**, L533 (2000).
[47] T. Graf, J. D. Thompson, M. F. Hundley, R. Movshovich, Z. Fisk, D. Mandrus, R. A. Fisher, and N. E. Phillips, Phys. Rev. Lett. **78**, 3769 (1997).
[48] R. Settai, A. Misawa, S. Araki, M. Kosaki, K. Sugiyama, T. Takeuchi, K. Kindo, Y. Haga, E. Yamamoto, and Y. Ōnuki, J. Phys. Soc. Jpn. **66**, 2260 (1997).
[49] S. Araki, M. Nakashima, R. Settai, T. C. Kobayashi, and Y. Ōnuki, J. Phys. Condens. Matter **14**, L377 (2002).
[50] Y. J. Uemura, W. J. Kossler, X. H. Yu, H. E. Schone, J. R. Kempton, C. E. Stronach, S. Barth, F. N. Gygax, B. Hitti, A. Schenck, et al., Phys. Rev. B **39**, 4726 (1989).
[51] O. Stockert, J. Arndt, A. Schneidewind, H. Schneider, H. S. Jeevan, C. Geibel, F. Steglich, and M. Loewenhaupt, Physica B **403**, 973 (2008).

[52] W. Assmus, M. Herrmann, U. Rauchschwalbe, S. Riegel, W. Lieke, H. Spille, S. Horn, G. Weber, F. Steglich, and G. Cordier, Phys. Rev. Lett. **52**, 469 (1984).

[53] F. R. de Boer, J. C. P. Klaasse, P. A. Veenhuizen, A. Böhm, C. D. Bredl, U. Gottwick, H. M. Mayer, L. Pawlak, U. Rauchschwalbe, H. Spille, et al., J. Magn. Magn. Mater. **63**, 91 (1987).

[54] G. Knopp, A. Loidl, K. Knorr, L. Pawlak, M. Duczmal, R. Caspary, U. Gottwick, H. Spille, F. Steglich, and A. P. Murani, Z. Phys. B **77**, 95 (1989).

[55] D. Jaccard, K. Behnia, and J. Sierro, Phys. Lett. A **163**, 475 (1992).

[56] Y. Ota, K. Sugiyama, Y. Miyauchi, Y. Takeda, Y. Nakano, Y. Doi, K. Katayama, N. D. Dung, T. D. Matsuda, Y. Haga, et al., J. Phys. Soc. Jpn. **78**, 034714 (2009).

[57] Z. Ren, L. V. Pourovskii, G. Giriat, G. Lapertot, A. Georges, and D. Jaccard, Phys. Rev. X **4**, 031055 (2014).

[58] E. D. Bauer, H. O. Lee, V. A. Sidorov, N. Kurita, K. Gofryk, J.-X. Zhu, F. Ronning, R. Movshovich, J. D. Thompson, and T. Park, Phys. Rev. B **81**, 180507 (2010).

[59] V. A. Sidorov, X. Lu, T. Park, H. Lee, P. H. Tobash, R. E. Baumbach, F. Ronning, E. D. Bauer, and J. D. Thompson, Phys. Rev. B **88**, 020503 (2013).

[60] S. E. Sebastian, N. Harrison, C. D. Batista, S. A. Trugman, V. Fanelli, M. Jaime, T. P. Murphy, E. C. Palm, H. Harima, and T. Ebihara, Proc. Natl. Acad. Sci. USA **106**, 7741 (2009).

[61] J. M. Lawrence and S. M. Shapiro, Phys. Rev. B **22**, 4379 (1980).

[62] A. Benoit, J. Boucherle, P. Convert, J. Flouquet, J. Palleau, and J. Schweizer, Solid State Commun. **34**, 293 (1980).

[63] G. Knebel, D. Braithwaite, P. Canfield, G. Lapertot, and J. Flouquet, High Pressure Res. **22**, 167 (2002).

[64] G. Knebel, D. Braithwaite, P. C. Canfield, G. Lapertot, and J. Flouquet, Phys. Rev. B **65**, 024425 (2001).

[65] C. Petrovic, P. G. Pagliuso, M. F. Hundley, R. Movshovich, J. L. Sarrao, J. D. Thompson, Z. Fisk, and P. Monthoux, J. Phys. Condens. Matter **13**, L337 (2001).

[66] L. Howald, G. Knebel, D. Aoki, G. Lapertot, and J.-P. Brison, New J. Phys. **13**, 113039 (2011).

[67] H. Hegger, C. Petrovic, E. G. Moshopoulou, M. F. Hundley, J. L. Sarrao, Z. Fisk, and J. D. Thompson, Phys. Rev. Lett. **84**, 4986 (2000).

[68] W. Bao, P. G. Pagliuso, J. L. Sarrao, J. D. Thompson, Z. Fisk, J. W. Lynn, and R. W. Erwin, Phys. Rev. B **62**, R14621 (2000).

[69] G. Knebel, D. Aoki, J.-P. Brison, and J. Flouquet, J. Phys. Soc. Jpn. **77**, 114704 (2008).

[70] Y. Ida, R. Settai, Y. Ota, F. Honda, and Y. Ōnuki, J. Phys. Soc. Jpn. **77**, 084708 (2008).

[71] C. Petrovic, R. Movshovich, M. Jaime, P. G. Pagliuso, M. F. Hundley, J. L. Sarrao, Z. Fisk, and J. D. Thompson, Europhys. Lett. **53**, 354 (2001).

[72] G. Chen, S. Ohara, M. Hedo, Y. Uwatoko, K. Saito, M. Sorai, and I. Sakamoto, J. Phys. Soc. Jpn. **71**, 2836 (2002).

[73] M. Hedo, N. Kurita, Y. Uwatoko, G. Chen, S. Ohara, and I. Sakamoto, J. Magn. Magn. Mater. **272-276**, 146 (2004).

[74] J. Thompson, R. Movshovich, Z. Fisk, F. Bouquet, N. Curro, R. Fisher, P. Hammel, H. Hegger, M. Hundley, M. Jaime, et al., J. Magn. Magn. Mater. **226-230**, 5 (2001).

[75] W. Bao, P. G. Pagliuso, J. L. Sarrao, J. D. Thompson, Z. Fisk, and J. W. Lynn, Phys. Rev. B **64**, 020401 (2001).

[76] M. Nicklas, V. A. Sidorov, H. A. Borges, P. G. Pagliuso, C. Petrovic, Z. Fisk, J. L. Sarrao, and J. D. Thompson, Phys. Rev. B **67**, 020506 (2003).

[77] D. Kaczorowski, A. P. Pikul, D. Gnida, and V. H. Tran, Phys. Rev. Lett. **103**, 027003 (2009).

[78] Y. Tokiwa, P. Gegenwart, D. Gnida, and D. Kaczorowski, Phys. Rev. B **84**, 140507 (2011).

[79] E. Bauer, G. Hilscher, H. Michor, C. Paul, E. W. Scheidt, A. Gribanov, Y. Seropegin, H. Noël, M. Sigrist, and P. Rogl, Phys. Rev. Lett. **92**, 027003 (2004).

[80] K. Kaneko, O. Stockert, M. Skoulatos, A. Schneidewind, T. Takeuchi, T. D. Matsuda, Y. Haga, R. Settai, Y. Ōnuki, and N. Metoki, J. Phys. Soc. Jpn. **81**, SB006 (2012).

[81] T. Yasuda, H. Shishido, T. Ueda, S. Hashimoto, R. Settai, T. Takeuchi, T. D. Matsuda, Y. Haga, and Y. Ōnuki, J. Phys. Soc. Jpn. **73**, 1657 (2004).

[82] V. K. Pecharsky, O.-B. Hyun, and K. A. Gschneidner, Phys. Rev. B **47**, 11839 (1993).

[83] M. Smidman, D. T. Adroja, A. D. Hillier, L. C. Chapon, J. W. Taylor, V. K. Anand, R. P. Singh, M. R. Lees, E. A. Goremychkin, M. M. Koza, et al., Phys. Rev. B **88**, 134416 (2013).

[84] R. Settai, I. Sugitani, Y. Okuda, A. Thamizhavel, M. Nakashima, Y. Ōnuki, and H. Harima, J. Magn. Magn. Mater. **310**, 844 (2007).

[85] M.-A. Méasson, H. Muranaka, T. Kawai, Y. Ota, K. Sugiyama, M. Hagiwara, K. Kindo, T. Takeuchi, K. Shimizu, F. Honda, et al., J. Phys. Soc. Jpn. **78**, 124713 (2009).

[86] Y. Muro, D. Eom, N. Takeda, and M. Ishikawa, J. Phys. Soc. Jpn. **67**, 3601 (1998).

[87] N. Kimura, Y. Muro, and H. Aoki, J. Phys. Soc. Jpn. **76**, 051010 (2007).

[88] N. Aso, H. Miyano, H. Yoshizawa, N. Kimura, T. Komatsubara, and H. Aoki, J. Magn. Magn. Mater. **310**, 602 (2007).

[89] N. Egetenmeyer, J. L. Gavilano, A. Maisuradze, S. Gerber, D. E. MacLaughlin, G. Seyfarth, D. Andreica, A. Desilets-Benoit, A. D. Bianchi, C. Baines, et al., Phys. Rev. Lett. **108**, 177204 (2012).

[90] N. Kimura, K. Ito, H. Aoki, S. Uji, and T. Terashima, Phys. Rev. Lett. **98**, 197001 (2007).

[91] N. Aso, M. Takahashi, H. Yoshizawa, H. Iida, N. Kimura, and H. Aoki, J. Phys.: Conf. Ser. **400**, 022003 (2012).

[92] I. Sugitani, Y. Okuda, H. Shishido, T. Yamada, A. Thamizhavel, E. Yamamoto, T. D. Matsuda, Y. Haga, T. Takeuchi, R. Settai, et al., J. Phys. Soc. Jpn. **75**, 043703 (2006).

[93] R. Settai, Y. Miyauchi, T. Takeuchi, F. Lévy, I. Sheikin, and Y. Ōnuki, J. Phys. Soc. Jpn. **77**, 073705 (2008).

[94] F. Honda, I. Bonalde, K. Shimizu, S. Yoshiuchi, Y. Hirose, T. Nakamura, R. Settai, and Y. Ōnuki, Phys. Rev. B **81**, 140507 (2010).

[95] D. Jérome, Science **252**, 1509 (1991).

[96] L. P. Gor'kov and E. I. Rashba, Phys. Rev. Lett. **87**,

037004 (2001).
[97] F. Steglich, P. Gegenwart, C. Geibel, R. Helfrich, P. Hellmann, M. Lang, A. Link, R. Modler, G. Sparn, N. Büttgen, et al., Physica B **223 - 224**, 1 (1996).
[98] O. Stockert, J. Arndt, E. Faulhaber, C. Geibel, H. S. Jeevan, S. Kirchner, M. Loewenhaupt, K. Schmalzl, W. Schmidt, Q. Si, et al., Nature Physics **7**, 119 (2011).
[99] S. Seiro, M. Deppe, H. Jeevan, U. Burkhardt, and C. Geibel, physica status solidi (b) **247**, 614 (2010).
[100] G. M. Luke, A. Keren, K. Kojima, L. P. Le, B. J. Sternlieb, W. D. Wu, Y. J. Uemura, Y. Ōnuki, and T. Komatsubara, Phys. Rev. Lett. **73**, 1853 (1994).
[101] R. Feyerherm, A. Amato, C. Geibel, F. N. Gygax, P. Hellmann, R. H. Heffner, D. E. MacLaughlin, R. Müller-Reisener, G. J. Nieuwenhuys, A. Schenck, et al., Phys. Rev. B **56**, 699 (1997).
[102] U. Rauchschwalbe, U. Ahlheim, F. Steglich, D. Rainer, and J. J. M. Franse, Z. Phys. B **60**, 379 (1985).
[103] K. Ueda, Y. Kitaoka, H. Yamada, Y. Kohori, T. Kohara, and K. Asayama, J. Phys. Soc. Jpn. **56**, 867 (1987).
[104] Y. Kitaoka, K. Ueda, T. Kohara, K. Asayama, Y. Ōnuki, and T. Komatsubara, J. Magn. Magn. Mater. **52**, 341 (1985).
[105] K. Ishida, Y. Kawasaki, K. Tabuchi, K. Kashima, Y. Kitaoka, K. Asayama, C. Geibel, and F. Steglich, Phys. Rev. Lett. **82**, 5353 (1999).
[106] I. Eremin, G. Zwicknagl, P. Thalmeier, and P. Fulde, Phys. Rev. Lett. **101**, 187001 (2008).
[107] H. A. Vieyra, N. Oeschler, S. Seiro, H. S. Jeevan, C. Geibel, D. Parker, and F. Steglich, Phys. Rev. Lett. **106**, 207001 (2011).
[108] S. Kittaka, Y. Aoki, Y. Shimura, T. Sakakibara, S. Seiro, C. Geibel, F. Steglich, H. Ikeda, and K. Machida, Phys. Rev. Lett. **112**, 067002 (2014).
[109] M. Enayat, Z. Sun, A. Maldonado, H. Suderow, S. Seiro, C. Geibel, S. Wirth, F. Steglich, and P. Wahl, Phys. Rev. B **93**, 045123 (2016).
[110] H. Ikeda, M.-T. Suzuki, and R. Arita, Phys. Rev. Lett. **114**, 147003 (2015).
[111] G. M. Pang, M. Smidman, J. L. Zhang, L. Jiao, Z. F. Weng, E. M. Nica, Y. Chen, W. B. Jiang, Y. J. Zhang, H. S. Jeevan, et al., arXiv:1605.04786 (2016).
[112] S. Kawasaki, M. Yashima, Y. Kitaoka, K. Takeda, K. Shimizu, Y. Oishi, M. Takata, T. C. Kobayashi, H. Harima, S. Araki, et al., Phys. Rev. B **77**, 064508 (2008).
[113] J. L. Sarrao and J. D. Thompson, J. Phys. Soc. Jpn. **76**, 051013 (2007).
[114] J. D. Thompson and Z. Fisk, J. Phys. Soc. Jpn. **81**, 011002 (2012).
[115] V. A. Sidorov, M. Nicklas, P. G. Pagliuso, J. L. Sarrao, Y. Bang, A. V. Balatsky, and J. D. Thompson, Phys. Rev. Lett. **89**, 157004 (2002).
[116] T. Park and J. D. Thompson, New J. Phys. **11**, 055062 (2009).
[117] A. Tursina, S. Nesterenko, Y. Seropegin, H. Noël, and D. Kaczorowski, J. Solid State Chem. **200**, 7 (2013).
[118] M. Kratochvílová, J. Prokleška, K. Uhlířová, V. Tkáč, M. Dušek, V. Sechovskỳ, and J. Custers, Sci. Rep. **5**, 15904 (2015).
[119] A. Severing, E. Holland-Moritz, and B. Frick, Phys. Rev. B **39**, 4164 (1989).
[120] N. Kernavanois, S. Raymond, E. Ressouche, B. Grenier, J. Flouquet, and P. Lejay, Phys. Rev. B **71**, 064404 (2005).
[121] I. Sheikin, A. Gröger, S. Raymond, D. Jaccard, D. Aoki, H. Harima, and J. Flouquet, Physica B **346-347**, 310 (2004).
[122] P. Gegenwart, F. Kromer, M. Lang, G. Sparn, C. Geibel, and F. Steglich, Phys. Rev. Lett. **82**, 1293 (1999).
[123] R. Küchler, P. Gegenwart, C. Geibel, and F. Steglich, Sci. Tech. Adv. Mater. **8**, 428 (2007).
[124] G. Knebel, M. Brando, J. Hemberger, M. Nicklas, W. Trinkl, and A. Loidl, Phys. Rev. B **59**, 12390 (1999).
[125] C. H. Wang, L. Poudel, A. E. Taylor, J. M. Lawrence, A. D. Christianson, S. Chang, J. A. Rodriguez-Rivera, J. W. Lynn, A. A. Podlesnyak, G. Ehlers, et al., J. Phys. Condens. Matter **27**, 015602 (2015).
[126] S. Kawasaki, T. Sada, T. Miyoshi, H. Kotegawa, H. Mukuda, Y. Kitaoka, T. C. Kobayashi, T. Fukuhara, K. Maezawa, K. M. Itoh, et al., J. Phys. Soc. Jpn. **75**, 043702 (2006).
[127] T. Graf, M. F. Hundley, R. Modler, R. Movshovich, J. D. Thompson, D. Mandrus, R. A. Fisher, and N. E. Phillips, Phys. Rev. B **57**, 7442 (1998).
[128] S. Kawarazaki, M. Sato, Y. Miyako, N. Chigusa, K. Watanabe, N. Metoki, Y. Koike, and M. Nishi, Phys. Rev. B **61**, 4167 (2000).
[129] R. Movshovich, T. Graf, D. Mandrus, J. D. Thompson, J. L. Smith, and Z. Fisk, Phys. Rev. B **53**, 8241 (1996).
[130] S. Araki, R. Settai, T. C. Kobayashi, H. Harima, and Y. Ōnuki, Phys. Rev. B **64**, 224417 (2001).
[131] A. Villaume, D. Aoki, Y. Haga, G. Knebel, R. Boursier, and J. Flouquet, J. Phys. Condens. Matter **20**, 015203 (2008).
[132] W. Knafo, D. Aoki, D. Vignolles, B. Vignolle, Y. Klein, C. Jaudet, A. Villaume, C. Proust, and J. Flouquet, Phys. Rev. B **81**, 094403 (2010).
[133] N. Metoki, K. Kaneko, T. D. Matsuda, A. Galatanu, T. Takeuchi, S. Hashimoto, T. Ueda, R. Settai, Y. Ōnuki, and N. Bernhoeft, J. Phys. Condens. Matter **16**, L207 (2004).
[134] T. Willers, B. Fåk, N. Hollmann, P. O. Körner, Z. Hu, A. Tanaka, D. Schmitz, M. Enderle, G. Lapertot, L. H. Tjeng, et al., Phys. Rev. B **80**, 115106 (2009).
[135] N. Tateiwa, Y. Haga, T. D. Matsuda, S. Ikeda, T. Yasuda, T. Takeuchi, R. Settai, and Y. Ōnuki, J. Phys. Soc. Jpn. **74**, 1903 (2005).
[136] A. Amato, E. Bauer, and C. Baines, Phys. Rev. B **71**, 092501 (2005).
[137] A. D. Hillier, D. T. Adroja, P. Manuel, V. K. Anand, J. W. Taylor, K. A. McEwen, B. D. Rainford, and M. M. Koza, Phys. Rev. B **85**, 134405 (2012).
[138] T. Kawai, Y. Okuda, H. Shishido, A. Thamizhavel, T. D. Matsuda, Y. Haga, M. Nakashima, T. Takeuchi, M. Hedo, Y. Uwatoko, et al., J. Phys. Soc. Jpn. **76**, 014710 (2007).
[139] F. Honda, I. Bonalde, S. Yoshiuchi, Y. Hirose, T. Nakamura, K. Shimizu, R. Settai, and Y. Ōnuki, Physica C **470**, S543 (2010).
[140] T. Kawai, H. Muranaka, M.-A. Measson, T. Shimoda, Y. Doi, T. D. Matsuda, Y. Haga, G. Knebel, G. Lapertot, D. Aoki, et al., J. Phys. Soc. Jpn. **77**, 064716 (2008).
[141] T. Kawai, M. Nakashima, Y. Okuda, H. Shishido, T. Shimoda, T. D. Matsuda, Y. Haga, T. Takeuchi, M. Hedo, Y. Uwatoko, et al., J. Phys. Soc. Jpn. **76**, 166 (2007).
[142] M. Smidman, D. T. Adroja, E. A. Goremychkin, M. R.

Lees, D. M. Paul, and G. Balakrishnan, Phys. Rev. B **91**, 064419 (2015).
[143] N. Aso, M. Takahashi, H. Yoshizawa, H. Iida, N. Kimura, and H. Aoki, J. Phys. Soc. Jpn. **80**, 095004 (2011).
[144] T. Terashima, Y. Takahide, T. Matsumoto, S. Uji, N. Kimura, H. Aoki, and H. Harima, Phys. Rev. B **76**, 054506 (2007).
[145] T. Terashima, M. Kimata, S. Uji, T. Sugawara, N. Kimura, H. Aoki, and H. Harima, Phys. Rev. B **78**, 205107 (2008).
[146] T. Ohkochi, T. Toshimitsu, H. Yamagami, S.-i. Fujimori, A. Yasui, Y. Takeda, T. Okane, Y. Saitoh, A. Fujimori, Y. Miyauchi, et al., J. Phys. Soc. Jpn. **78**, 084802 (2009).
[147] N. Kimura, K. Ito, K. Saitoh, Y. Umeda, H. Aoki, and T. Terashima, Phys. Rev. Lett. **95**, 247004 (2005).
[148] T. Sugawara, H. Iida, H. Aoki, and N. Kimura, J. Phys. Soc. Jpn. **81**, 054711 (2012).
[149] A. Thamizhavel, T. Takeuchi, T. D. Matsuda, Y. Haga, K. Sugiyama, R. Settai, and Y. Ōnuki, J. Phys. Soc. Jpn. **74**, 1858 (2005).
[150] A. Thamizhavel, H. Shishido, Y. Okuda, H. Harima, T. D. Matsuda, Y. Haga, R. Settai, and Y. Ōnuki, J. Phys. Soc. Jpn. **75**, 044711 (2006).
[151] I. Sheikin, P. Rodiere, R. Settai, and Y. Ōnuki, J. Phys. Soc. Jpn. **80**, SA020 (2011).
[152] K. Kaneko, N. Metoki, T. Takeuchi, T. D. Matsuda, Y. Haga, A. Thamizhavel, R. Settai, and Y. Ōnuki, J. Phys.: Conf. Ser. **150**, 042082 (2009).
[153] A. Das, R. K. Kremer, R. Pöttgen, and B. Ouladdiaf, Physica B **378-380**, 837 (2006).
[154] M. Mizoo, T. Nishioka, H. Kato, and M. Matsumura, J. Phys.: Conf. Ser. **273**, 012009 (2011).
[155] G. Knebel, D. Aoki, G. Lapertot, B. Salce, J. Flouquet, T. Kawai, H. Muranaka, R. Settai, and Y. Ōnuki, J. Phys. Soc. Jpn. **78**, 074714 (2009).
[156] K. Izawa, Y. Kasahara, Y. Matsuda, K. Behnia, T. Yasuda, R. Settai, and Y. Ōnuki, Phys. Rev. Lett. **94**, 197002 (2005).
[157] I. Bonalde, W. Brämer-Escamilla, and E. Bauer, Phys. Rev. Lett. **94**, 207002 (2005).
[158] H. Mukuda, T. Fujii, T. Ohara, A. Harada, M. Yashima, Y. Kitaoka, Y. Okuda, R. Settai, and Y. Ōnuki, Phys. Rev. Lett. **100**, 107003 (2008).
[159] P. A. Frigeri, D. F. Agterberg, and M. Sigrist, New J. Phys. **6**, 115 (2004).
[160] H. Mukuda, T. Ohara, M. Yashima, Y. Kitaoka, R. Settai, Y. Ōnuki, K. M. Itoh, and E. E. Haller, Phys. Rev. Lett. **104**, 017002 (2010).
[161] M. Yogi, Y. Kitaoka, S. Hashimoto, T. Yasuda, R. Settai, T. D. Matsuda, Y. Haga, Y. Ōnuki, P. Rogl, and E. Bauer, Phys. Rev. Lett. **93**, 027003 (2004).
[162] F. Thomas, J. Thomasson, C. Ayache, C. Geibel, and F. Steglich, Physica B **186**, 303 (1993).
[163] D. Jaccard, H. Wilhelm, K. Alami-Yadri, and E. Vargoz, Physica B **259-261**, 1 (1999).
[164] F. Thomas, C. Ayache, I. A. Fomine, J. Thomasson, and C. Geibel, J. Phys. Condens. Matter **8**, L51 (1996).
[165] H. Ikeda, J. Phys. Soc. Jpn. **71**, 1126 (2002).
[166] H. Q. Yuan, M. Deppe, G. Sparn, C. Geibel, and F. Steglich, Acta Physica Polonica B **34**, 533 (2003).
[167] H. Q. Yuan, F. M. Grosche, M. Deppe, G. Sparn, C. Geibel, and F. Steglich, Phys. Rev. Lett. **96**, 047008 (2006).
[168] H. Q. Yuan, F. M. Grosche, M. Deppe, C. Geibel, G. Sparn, and F. Steglich, New J. Phys. **6**, 132 (2004).
[169] A. Onodera, S. Tsuduki, Y. Ohishi, T. Watanuki, K. Ishida, Y. Kitaoka, and Y. Ōnuki, Solid State Commun. **123**, 113 (2002).
[170] J.-P. Rueff, S. Raymond, M. Taguchi, M. Sikora, J.-P. Itié, F. Baudelet, D. Braithwaite, G. Knebel, and D. Jaccard, Phys. Rev. Lett. **106**, 186405 (2011).
[171] H. Yamaoka, Y. Ikeda, I. Jarrige, N. Tsujii, Y. Zekko, Y. Yamamoto, J. Mizuki, J.-F. Lin, N. Hiraoka, H. Ishii, et al., Phys. Rev. Lett. **113**, 086403 (2014).
[172] T. Willers, F. Strigari, N. Hiraoka, Y. Q. Cai, M. W. Haverkort, K.-D. Tsuei, Y. F. Liao, S. Seiro, C. Geibel, F. Steglich, et al., Phys. Rev. Lett. **109**, 046401 (2012).
[173] K. Hattori, J. Phys. Soc. Jpn. **79**, 114717 (2010).
[174] L. V. Pourovskii, P. Hansmann, M. Ferrero, and A. Georges, Phys. Rev. Lett. **112**, 106407 (2014).
[175] J.-P. Rueff, J. M. Ablett, F. Strigari, M. Deppe, M. W. Haverkort, L. H. Tjeng, and A. Severing, Phys. Rev. B **91**, 201108 (2015).
[176] S. Kawasaki, M. Yashima, Y. Mugino, H. Mukuda, Y. Kitaoka, H. Shishido, and Y. Ōnuki, Phys. Rev. Lett. **96**, 147001 (2006).
[177] M. Nicklas, V. A. Sidorov, H. A. Borges, P. G. Pagliuso, J. L. Sarrao, and J. D. Thompson, Phys. Rev. B **70**, 020505 (2004).
[178] E. D. Bauer, M. M. Altarawneh, P. H. Tobash, K. Gofryk, O. E. Ayala-Valenzuela, J. N. Mitchell, R. D. McDonald, C. H. Mielke, F. Ronning, J.-C. Griveau, et al., J. Phys. Condens. Matter **24**, 052206 (2012).
[179] S. Kawasaki, G.-q. Zheng, H. Kan, Y. Kitaoka, H. Shishido, and Y. Ōnuki, Phys. Rev. Lett. **94**, 037007 (2005).
[180] P. G. Pagliuso, C. Petrovic, R. Movshovich, D. Hall, M. F. Hundley, J. L. Sarrao, J. D. Thompson, and Z. Fisk, Phys. Rev. B **64**, 100503 (2001).
[181] T. Shang, R. E. Baumbach, K. Gofryk, F. Ronning, Z. F. Weng, J. L. Zhang, X. Lu, E. D. Bauer, J. D. Thompson, and H. Q. Yuan, Phys. Rev. B **89**, 041101 (2014).
[182] T. Willers, F. Strigari, Z. Hu, V. Sessi, N. B. Brookes, E. D. Bauer, J. L. Sarrao, J. D. Thompson, A. Tanaka, S. Wirth, et al., Proc. Natl. Acad. Sci. USA **112**, 2384 (2015).
[183] A. McMahan, C. Huscroft, R. Scalettar, and E. Pollock, J. Comput. Aided Mater. Des. **5**, 131 (1998).
[184] A. Chatterjee, A. K. Singh, and A. Jayaraman, Phys. Rev. B **6**, 2285 (1972).
[185] J. M. De Teresa, Z. Arnold, A. del Moral, M. R. Ibarra, J. Kamarád, D. T. Adroja, and B. Rainford, Solid State Commun. **99**, 911 (1996).
[186] J. L. Sarrao, A. P. Ramirez, T. W. Darling, F. Freibert, A. Migliori, C. D. Immer, Z. Fisk, and Y. Uwatoko, Phys. Rev. B **58**, 409 (1998).
[187] T. Park, V. A. Sidorov, J. L. Sarrao, and J. D. Thompson, Phys. Rev. Lett. **96**, 046405 (2006).
[188] W. B. Jiang, L. Yang, C. Y. Guo, Z. Hu, J. M. Lee, M. Smidman, Y. F. Wang, T. Shang, Z. W. Cheng, F. Gao, et al., Sci. Rep. **5**, 17608 (2015).
[189] H. V. Löhneysen, J. Phys. Condens. Matter **8**, 9689 (1996).
[190] P. Wölfle and E. Abrahams, Phys. Rev. B **84**, 041101 (2011).

[191] S. Watanabe and K. Miyake, Phys. Rev. Lett. **105**, 186403 (2010).

[192] H. Shishido, R. Settai, H. Harima, and Y. Ōnuki, J. Phys. Soc. Jpn. **74**, 1103 (2005).

[193] Y. Ōnuki, Y. Shimizu, and T. Komatsubara, J. Phys. Soc. Jpn. **54**, 304 (1985).

[194] F. Steglich, U. Rauchschwalbe, U. Gottwick, H. M. Mayer, G. Sparn, N. Grewe, U. Poppe, and J. J. M. Franse, J. Appl. Phys. **57**, 3054 (1985).

[195] M. Klein, A. Nuber, F. Reinert, J. Kroha, O. Stockert, and H. v. Löhneysen, Phys. Rev. Lett. **101**, 266404 (2008).

[196] M. Klein, J. Kroha, H. v. Löhneysen, O. Stockert, and F. Reinert, Phys. Rev. B **79**, 075111 (2009).

[197] J. Kroha, M. Klein, A. Nuber, F. Reinert, O. Stockert, and H. v Löhneysen, J. Phys. Condens. Matter **22**, 164203 (2010).

[198] A. Schröder, G. Aeppli, R. Coldea, M. Adams, O. Stockert, H. v. Löhneysen, E. Bucher, R. Ramazashvili, and P. Coleman, Nature **407**, 351 (2000).

[199] H. v. Löhneysen, C. Pfleiderer, T. Pietrus, O. Stockert, and B. Will, Phys. Rev. B **63**, 134411 (2001).

[200] O. Stockert, M. Enderle, and H. v. Löhneysen, Phys. Rev. Lett. **99**, 237203 (2007).

[201] P. Gegenwart, J. Custers, C. Geibel, K. Neumaier, T. Tayama, K. Tenya, O. Trovarelli, and F. Steglich, Phys. Rev. Lett. **89**, 056402 (2002).

[202] J. Custers, P. Gegenwart, H. Wilhelm, K. Neumaier, Y. Tokiwa, O. Trovarelli, C. Geibel, F. Steglich, C. Pépin, and P. Coleman, Nature **424**, 524 (2003).

[203] S. Paschen, T. Lühmann, S. Wirth, P. Gegenwart, O. Trovarelli, C. Geibel, F. Steglich, P. Coleman, and Q. Si, Nature **432**, 881 (2004).

[204] S. Watanabe and K. Miyake, J. Phys. Soc. Jpn. **82**, 083704 (2013).

[205] A. Hackl and M. Vojta, Phys. Rev. Lett. **106**, 137002 (2011).

[206] S. Friedemann, T. Westerkamp, M. Brando, N. Oeschler, S. Wirth, P. Gegenwart, C. Krellner, C. Geibel, and F. Steglich, Nature Physics **5**, 465 (2009).

[207] H. Shishido, R. Settai, D. Aoki, S. Ikeda, H. Nakawaki, N. Nakamura, T. Iizuka, Y. Inada, K. Sugiyama, T. Takeuchi, et al., J. Phys. Soc. Jpn. **71**, 162 (2002).

[208] N. Harrison, U. Alver, R. G. Goodrich, I. Vekhter, J. L. Sarrao, P. G. Pagliuso, N. O. Moreno, L. Balicas, Z. Fisk, D. Hall, et al., Phys. Rev. Lett. **93**, 186405 (2004).

[209] T. Maehira, T. Hotta, K. Ueda, and A. Hasegawa, J. Phys. Soc. Jpn. **72**, 854 (2003).

[210] P. J. W. Moll, B. Zeng, L. Balicas, S. Galeski, F. F. Balakirev, E. D. Bauer, and F. Ronning, Nat. Comm. **6** (2015).

[211] H. Q. Yuan, *Unpublished results.* (2016).

[212] J. Custers, K.-A. Lorenzer, M. Müller, A. Prokofiev, A. Sidorenko, H. Winkler, A. M. Strydom, Y. Shimura, T. Sakakibara, R. Yu, et al., Nat. Mater. **11**, 189 (2012).

[213] Y. Luo, F. Ronning, N. Wakeham, X. Lu, T. Park, Z.-A. Xu, and J. D. Thompson, Proc. Natl. Acad. Sci. USA **112**, 13520 (2015).

[214] H. Li, Y. Liu, G.-M. Zhang, and L. Yu, J. Phys. Condens. Matter **27**, 425601 (2015).

[215] Y. Mizukami, H. Shishido, T. Shibauchi, M. Shimozawa, S. Yasumoto, D. Watanabe, M. Yamashita, H. Ikeda, T. Terashima, H. Kontani, et al., Nature Physics **7**, 849 (2011).

[216] S. K. Goh, Y. Mizukami, H. Shishido, D. Watanabe, S. Yasumoto, M. Shimozawa, M. Yamashita, T. Terashima, Y. Yanase, T. Shibauchi, et al., Phys. Rev. Lett. **109**, 157006 (2012).

[217] M. Shimozawa, S. K. Goh, R. Endo, R. Kobayashi, T. Watashige, Y. Mizukami, H. Ikeda, H. Shishido, Y. Yanase, T. Terashima, et al., Phys. Rev. Lett. **112**, 156404 (2014).

[218] H. Q. Yuan, D. F. Agterberg, N. Hayashi, P. Badica, D. Vandervelde, K. Togano, M. Sigrist, and M. B. Salamon, Phys. Rev. Lett. **97**, 017006 (2006).

[219] M. Smidman, M. B. Salamon, H. Q. Yuan, and D. F. Agterberg, Rep. Prog. Phys. Submitted (2016).